NAVAL POSTGRADUATE SCHOOL

MONTEREY, CALIFORNIA

THESIS

DETERMINATION OF SHOCK PROPERTIES OF CERAMIC CORBIT 98: 98% ALUMINA

by

Jeffrey R. Denzel

June 2010

Thesis Advisor:	Robert Hixson
Co-Advisor:	Jose Sinibaldi

Approved for public release; distribution is unlimited

THIS PAGE INTENTIONALLY LEFT BLANK

REPORT DOCUMENTATION PAGE			*Form Approved OMB No. 0704-0188*
Public reporting burden for this collection of information is estimated to average 1 hour per response, including the time for reviewing instruction, searching existing data sources, gathering and maintaining the data needed, and completing and reviewing the collection of information. Send comments regarding this burden estimate or any other aspect of this collection of information, including suggestions for reducing this burden, to Washington headquarters Services, Directorate for Information Operations and Reports, 1215 Jefferson Davis Highway, Suite 1204, Arlington, VA 22202-4302, and to the Office of Management and Budget, Paperwork Reduction Project (0704-0188) Washington DC 20503.			
1. AGENCY USE ONLY *(Leave blank)*	**2. REPORT DATE** June 2010	**3. REPORT TYPE AND DATES COVERED** Master's Thesis	
4. TITLE AND SUBTITLE Determination of the Shock Properties of Ceramic Corbit 98: 98% Alumina.		**5. FUNDING NUMBERS**	
6. AUTHOR(S) ENS Jeffrey R. Denzel, USN			
7. PERFORMING ORGANIZATION NAME(S) AND ADDRESS(ES) Naval Postgraduate School Monterey, CA 93943-5000		**8. PERFORMING ORGANIZATION REPORT NUMBER**	
9. SPONSORING /MONITORING AGENCY NAME(S) AND ADDRESS(ES) N/A		**10. SPONSORING/MONITORING AGENCY REPORT NUMBER**	
11. SUPPLEMENTARY NOTES The views expressed in this thesis are those of the author and do not reflect the official policy or position of the Department of Defense or the U.S. Government. IRB Protocol number ___N/A_____.			
12a. DISTRIBUTION / AVAILABILITY STATEMENT Approved for public release; distribution is unlimited		**12b. DISTRIBUTION CODE**	

13. ABSTRACT (maximum 200 words)

The shock properties of Bitossi Corbit 98 have been investigated. The Hugoniot Elastic Limit (HEL) was determined to be 7.96 ± 1.5 and 8.27 ± 0.8 GPa in two separate experiments. The strength in tension was found to be 0.271 GPa. The Hugoniot equation of state for elastic compression was calculated to be: Us=0.936*Up+10.53

This ceramic material—98% Al2O3—has been selected as the first component in a new layered armor design, which requires knowledge of the information discussed. The design encompasses an extremely hard first layer to deform the projectile, an orthotropic second layer to slow down the shock wave propagation, a third porous layer to absorb the shock wave energy through PV-work, and a fourth layer to provide confinement for the porous medium. Shock properties were determined by parallel plate impact experiments done at various velocities: 200-800m/s. The impactor material for asymmetric experiments was sapphire or aluminum. A single stage three inch bore gas gun was used to accelerate the projectile for experiments at NPS. Los Alamos National Lab used a higher performance gun to obtain higher impact speeds. A velocity interferometer was used to determine shock velocity in combination with time of arrival pins. These results confirmed previous work at higher pressures. Through this study, improved data for this ceramic were obtained, which will allow higher fidelity numeric simulations of overall armor system performance to be done.

14. SUBJECT TERMS Ceramic, Shock properties, Hugoniot equation of state, Hugoniot elastic limit, sound speed, single stage gas gun.			**15. NUMBER OF PAGES** 95
			16. PRICE CODE
17. SECURITY CLASSIFICATION OF REPORT Unclassified	**18. SECURITY CLASSIFICATION OF THIS PAGE** Unclassified	**19. SECURITY CLASSIFICATION OF ABSTRACT** Unclassified	**20. LIMITATION OF ABSTRACT** UU

NSN 7540-01-280-5500 Standard Form 298 (Rev. 2-89)
Prescribed by ANSI Std. 239-18

THIS PAGE INTENTIONALLY LEFT BLANK

Approved for public release; distribution is unlimited

DETERMINATION OF SHOCK PROPERTIES OF CERAMIC CORBIT 98: 98% ALUMINA

Jeffrey R. Denzel
Ensign, United States Navy
B.S., United States Naval Academy, 2009

Submitted in partial fulfillment of the
requirements for the degree of

MASTER OF SCIENCE IN APPLIED PHYSICS

from the

NAVAL POSTGRADUATE SCHOOL
June 2010

Author: Jeffrey R. Denzel

Approved by: Professor Robert Hixson
Thesis Advisor

Professor Jose Sinibaldi
Co-Advisor

Professor Andres Larraza
Chairman, Department of Physics

THIS PAGE INTENTIONALLY LEFT BLANK

ABSTRACT

The shock properties of Bitossi Corbit 98 have been investigated. The Hugoniot Elastic Limit (HEL) was determined to be 7.96 ± 1.5 and 8.27 ± 0.8 GPa in two separate experiments. The strength in tension was found to be 0.271 GPa. The Hugoniot equation of state for elastic compression was calculated to be: Us=0.936*Up+10.53

This ceramic material—98% Al2O3—has been selected as the first component in a new layered armor design, which requires knowledge of the information discussed. The design encompasses an extremely hard first layer to deform the projectile, an orthotropic second layer to slow down the shock wave propagation, a third porous layer to absorb the shock wave energy through PV-work, and a fourth layer to provide confinement for the porous medium. Shock properties were determined by parallel plate impact experiments done at various velocities: 200-800m/s. The impactor material for asymmetric experiments was sapphire or aluminum. A single stage three inch bore gas gun was used to accelerate the projectile for experiments at NPS. Los Alamos National Lab used a higher performance gun to obtain higher impact speeds. A velocity interferometer was used to determine shock velocity in combination with time of arrival pins. These results confirmed previous work at higher pressures. Through this study, improved data for this ceramic were obtained, which will allow higher fidelity numeric simulations of overall armor system performance to be done.

THIS PAGE INTENTIONALLY LEFT BLANK

TABLE OF CONTENTS

LIST OF FIGURES

THIS PAGE INTENTIONALLY LEFT BLANK

LIST OF TABLES

THIS PAGE INTENTIONALLY LEFT BLANK

LIST OF ACRONYMS AND ABBREVIATIONS

AL6061	Aluminum alloy 6061
EFP	Explosively formed projectiles
g/cc	gram per cubic centimeter
GPa	Gigapascals, one billion pascals of pressure or force per unit area
HEL	Hugoniot elastic limit
LANL	Los Alamos National Lab
mm	Millimeter, or one thousandth of a meter
mrad	Milliradians, or one thousandth of a radian angle measurement
ms	Milliseconds, or one thousandth of a second
NPS	Naval Postgraduate School
ns	nanosecond, one billionth of a second
PDV	photonic Doppler velocimetry
PSI	pounds per square inch
PZT	piezoelectric
RHA	Rolled Homogeneous Armor
SNL	Sandia National Lab
VISAR	Velocity interferometer system for any reflector
μm	Micrometer, one millionth of a meter
μs	Microsecond, one millionth of a second

THIS PAGE INTENTIONALLY LEFT BLANK

ACKNOWLEDGMENTS

First and foremost, I would like to thank my research advisors for showing me the ropes and providing support through my academic journey. Without their guidance, I would not have been able to achieve success in such a short window of time.

Next, I would like to thank the support staff for providing me with those crucial thousandths of an inch that make or break a shot experiment. Thank you, George and Sam.

Of course, none of this would have been possible without the funding provided by the Office of Naval Research. I simply cannot thank Brian Jensen at LANL enough for firing shots out in New Mexico.

Last, but certainly not least, I must acknowledge my family's contribution of enabling me to maintain my sanity over the past year. This tour has been my briefest and most pleasant.

THIS PAGE INTENTIONALLY LEFT BLANK

I. INTRODUCTION

A. BACKGROUND

This thesis is a focused continuation of previous Naval Postgraduate School (NPS) research performed in 2009 by Ong [1] and Poh [2] to investigate the utility of using a layered structure for personnel armor, using fundamental physics concepts. Each of the four components in the structure serves a basic purpose: first, plastically deforming the projectile; second, spreading out the shock wave; third, absorbing energy; lastly, preventing penetration. In order to accurately validate this model, the shock properties of the first material will be investigated.

Obtaining fundamental information that will lead to a better understanding of how a material absorbs and dissipates energy from an incoming projectile is the basic impetus of this work, as is spreading out the time rate of delivery of momentum. When an impact occurs, shock waves are immediately generated and propagate through both the impacting material and the target materials. Unique shock properties define each material. These shock properties are crucial in analyzing the utility of a given material for armor applications.

The critical transition between elastic (recoverable) and plastic (irrevocable) deformation is known as the Hugoniot elastic limit (HEL). This is the point at which a material loses some of its ability to resist penetration—namely it loses its ability to support shear stress. This is important in the penetration process because an armor material with very high strength will cause significant deformation to occur in the projectile, rather than in the armor. Plastic deformation causes projectile kinetic energy to be converted into internal energy and dissipated as heat. This in turn decreases the possibility of complete penetration. Therefore, a good material for the first layer of a composite armor material would be a material with a very high Hugoniot elastic limit (HEL). The most appealing characteristic of Corbit 98, the ceramic used in this body of work, is its potentially very high HEL. The HEL of this ceramic is nearly ten times that of steel. For this reason, it was selected as the first layer of a new layered armor concept.

One primary goal of our research was to experimentally determine the HEL of Corbit-98. The use of a layered armor system with each layer tuned to its application may allow an innovative change in the way armor plates are currently designed. Potential space and weight savings are anticipated with associated better specific (per unit mass) penetration resistance abilities.

The purpose of this study was to investigate a new concept in armor plate technology based on fundamental shock physics to stop a projectile penetration in a series of stages:

Stage 1: Momentum Dispersion is accomplished by using high yield strength, high impedance materials to resist penetration from compressive forces as much as possible and spread the momentum delivery out with time, thus, decreasing impulse. These materials cause significant deformation in the projectile, and so decrease its kinetic energy.

Stage 2: Wave Spreading is accomplished using special orthotropic composites, with very high lateral speed of sound to spread shock waves laterally away from the incident axis.

Stage 3: Energy Absorption takes place by using porous materials to convert kinetic energy into heat and through work done in compressing the pores of the material (PV-work).

Stage 4: Penetration Prevention is the goal of the final stopping layer. Should any projectile be able to penetrate through the first three layers, the final layer uses conventional means to prevent penetration of the target. This layer also provides required support for the porous layer.

Figure 1. displays this concept:

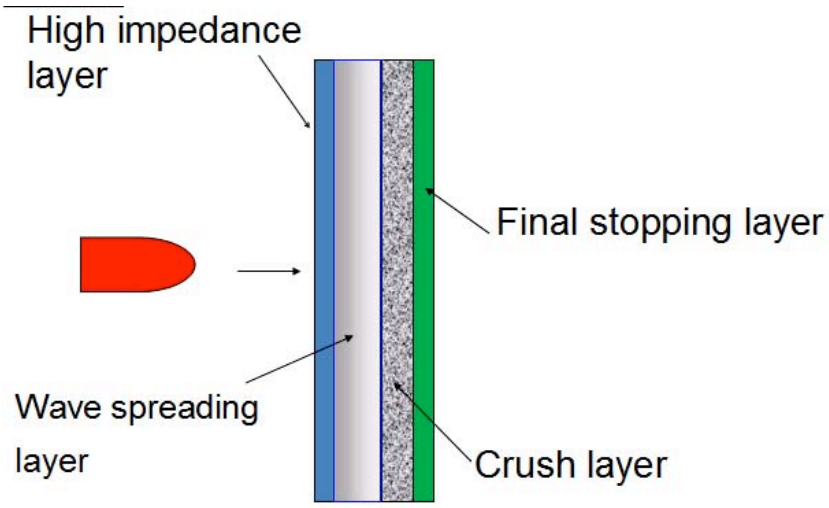

Figure 1. Graphical Illustration Of New Armor Layering Concept

B. LITERATURE RESEARCH

1. Ballistic Protection

Presently, much armor research is based on finding a single material that can resist penetration from projectiles and fragments. The standard is high strength steel called Rolled Homogeneous Armor (RHA), which is a hardened steel alloy with HEL ranging between 2 and 3 GPa. However, it is relatively simple to design weapons to defeat even the strongest steels. A significant issue with steel is its high density, making body armors impractical and bulky. To overcome this flaw, armors using brittle super-hard materials of lower density are employed. The upside is their strength exceeds steels by an order of magnitude or more. However, these materials do not offer direct multi-hit survivability because they are typically brittle and very weak in tension. For this reason, layered armors have become the emerging technology. These systems include Kevlar Fiber-Reinforced Polymers (KFRP), Carbon Fiber Reinforced Polymers (CFRP), and Aramid or Polyethylene woven fabric composites. Figure 2 shows a brief classification of these advanced composites. Such evolution of protection technology has had varying success in the defeat of some projectiles, depending upon the usage requirements. It is possible that the protection level for these existing technologies may have reached a plateau with marginal improvements within each spiral of armor development. Therefore,

a reasonable new direction is to use these new composite materials in a layered armor design with other materials that also have beneficial properties. This would include materials such as those discussed above that posses very high yield strength. Ceramics have been used in this application for some time, but new materials are under development. Such new materials include amorphous metallic alloys and other super-hard materials such as boron carbide.

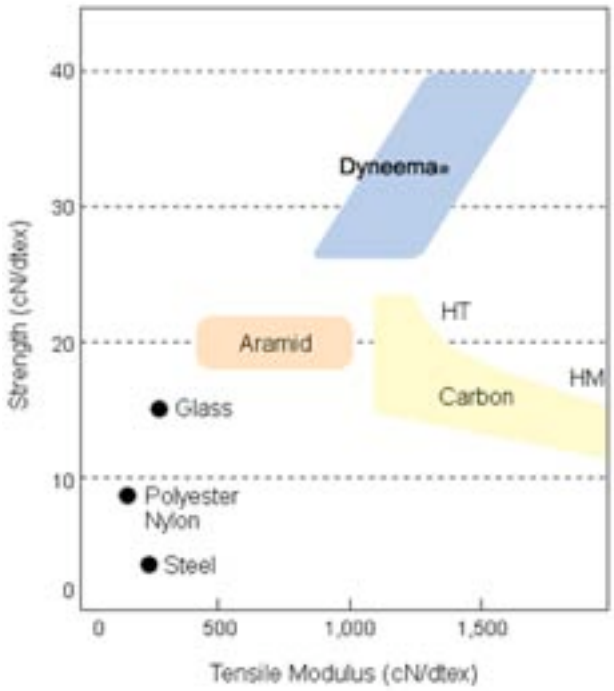

Figure 2. Relative Strength/ Tensile Modulus of Advanced Fiber Composites (From [1])

The horizontal axis describes tensile modulus, also known as Young's modulus. Young's modulus defines how elastic a material is. The units are in centi-Newtons per deci-tex, which is the load per unit line density. 1 deci-tex is the weight in grams of 10,000m of a single strand of fiber. The vertical axis represents strength in the same units.

2. Projectile Threats

Just as armor has evolved, offensive threats continue to adapt, perhaps even more quickly than defensive systems, and these are becoming readily available and widely distributed. Technology such as EFPs (explosively formed projectiles) and shaped charge jets are now easily designed and constructed (and unfortunately, put to use) by rogue nations and terrorist organizations alike. Many armors can be defeated by such threats due to fundamental physical effects. It is a continual challenge to evolve protective systems that can keep up with the evolution of threats.

3. Impetus for Ongoing Research

The need for the improvement of penetration protection is clear. Many, including Robbins et al. [3], have shown the feasibility of layered armor systems. Gupta et al. [4] demonstrated using a wave spreading material to dissipate the compressive forces of the incoming projectile, within a microsecond timescale. Wilkins et al. [5] have shown the effectiveness of ceramics in plastically deforming the projectile thus defeating it from the onset, preventing extensive damage to the lower layers of armor. Herrman [6] has also demonstrated the effectiveness of porous materials in absorbing energy due to shock compression. These are all relevant concepts which may lead to more effective armor. However, work has been lacking in putting these concepts together into a cohesive armor system.

Poh [2] has shown the feasibility of a composite layered construction made up of quite dissimilar materials each with specific properties to aid penetration resistance of the composite plate. It consists of a hard first layer to plastically defeat the projectile, and a multiple wave spreading layer to laterally dissipate the compressive shock waves. This is then followed by a porous layer to aid energy absorption. Numerical simulations using the Autodyn® hydrodynamic computer code have shown the benefits of having this sequence of layers to arrest the shock propagation due to a projectile impact, and it was predicted that this type of construction has the potential to outperform an AISI 4340 armor grade high strength steel plate of equivalent thickness. Figure 3 shows a 15mm length, 8mm diameter Tantalum cylinder penetrating completely through a 16mm thick

AISI 4340 16mm Steel Plate at an impact velocity of 1000m/s. The same projectile is completely stopped by a composite plate of the same thickness (16mm).

It is worthwhile to note that in this research we are primarily focused on the early time wave propagation of an impact event, and the ability to rapidly spread out the initial momentum of the projectile upon impact (μs timeframe) through fundamental shock physics theory, with the late time (millisecond timeframe) energy dissipation effects considered as a secondary objective. If dynamic properties of the relevant materials are captured correctly, a hydrodynamics computer code will be able to successfully calculate late time response.

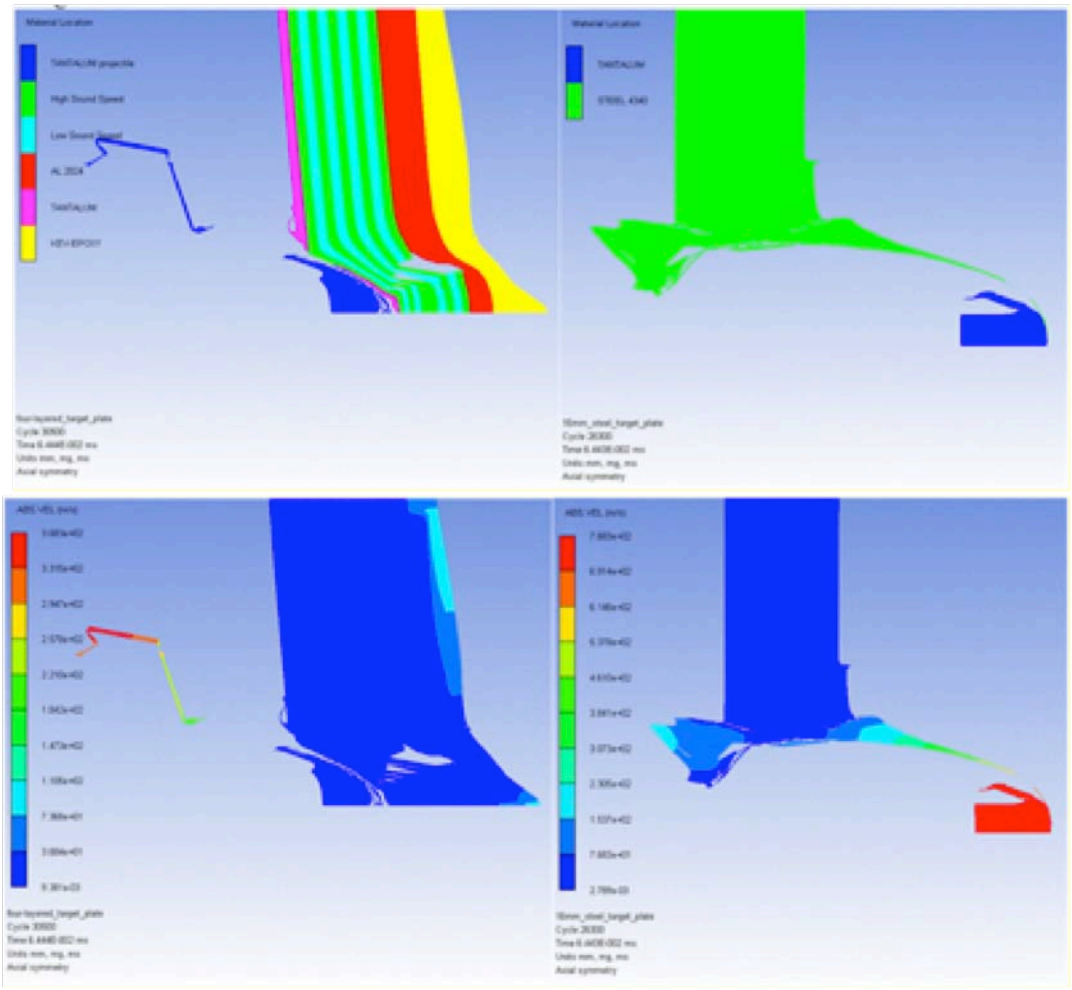

Figure 3. A composite plate construction was shown by Poh to defeat a projectile where a high strength AISI 4340 steel had failed

Anderson et al [7] reported a failure of the Drucker-Prager method to accurately model the dynamic response of ceramics and other brittle materials. This further supports the need to develop a method for computer simulations. The way to achieve this is to acquire critical material characteristics. That is the focus of this research.

4. Research Approach

In view of the novel challenges this project presents, a conservative and careful approach has been taken to reach the final recommendation. The investigation begins with an overview of shock physics, since we will use that technical approach to obtain the relevant high strain rate data. While this investigation is focused on ceramics, other components of the layered armor system, and potential alternatives for the high strength layer will also be discussed briefly. Alternatives to Al_2O_3 (alumina) based ceramics include silicon carbide, bulk amorphous alloys, boron carbides, and other materials. Several single stage gas gun experiments have been performed to acquire dynamic data that will be used to refine our existing computational approach. We will discuss experimental results, data analysis and final technical results. We will also discuss how the results of this work will allow refinement of our approach to calculation, and provide recommendations for future research.

THIS PAGE INTENTIONALLY LEFT BLANK

II. EXPERIMENTAL METHODS

A. INTRODUCTION TO SHOCK PHYSICS

All materials respond to impulsive loading in a way that depends upon the nature of the loading and intrinsic material properties. If we choose a simple loading geometry such as planar compression, we can measure certain fundamental properties. Since planar compression means that all volume change occurs in one direction, this is uniaxial strain loading, which allows us to simplify to some degree the stress and strain tensors. The zero pressure sound speed that is most relevant for this loading condition is the longitudinal sound speed. If shear wave velocity is also measured, then for isotropic materials all other elastic properties may then be found.

When the yield strength of the material of interest is exceeded, plastic flow will begin and elastic response is terminated. Because the ceramic material we are studying has a very high yield strength, we must measure both elastic and plastic material response to be able to constrain theoretical material models. The shock speeds produced by impact, when combined with material (particle) velocity define the shock 'Hugoniot.' One of the goals of our research is to measure this relationship to the highest stress state possible with our experimental apparatus.

The relationship between shock and particle velocity is linear for many materials over some finite stress regime. Sometimes this relationship is not linear, and this can signal the existence of some interesting phenomena. The equation of state relating shock speed to particle speed is known as the Hugoniot equation of state. For all materials with strength, there exist two Hugoniots. One is for elastic behavior and the other is for plastic behavior. However, for many materials the HEL is low enough that only the plastic Hugoniot needs to be considered. Since our chosen ceramic has a very high HEL we must consider both. In this work, the elastic response of our ceramic is carefully examined, as well as the HEL.

As previously mentioned, the HEL is the transition point between these two regimes. Many materials have relatively low values for the HEL, and so the elastic shock

speeds are very close to the longitudinal sound speed. But for materials with high elastic limit such as the ceramic material studied in this research the elastic wave is also expected to 'shock-up' and we expect to see shock velocity increase with increasing stress even for elastic states.

B. GAS GUN DESCRIPTION

1. Existing Gas Gun Facility

At the Naval Postgraduate School, the Impact Physics Lab is equipped with a 76mm (~3 in) bore single stage light gas gun. The light gas used is Helium, and at high pressures it can propel a projectile to relatively high velocities. By design, the gun achieves a desired speed by adjusting the breech pressure and the projectile mass. The breech is a 'wrap around' design and requires no diaphragms. Instead, there are o-rings at both ends of the projectile, which separate the high pressure in the breech from the rest of the gun. Prior to firing, the entire gun is pumped down to low vacuum—approximately 30 millitorr. To fire, a small jet of gas pushes on the back of the projectile, moving the rear o-ring past the breech ports. This allows gas stored in the reservoir to flow behind the projectile and accelerate it down the barrel. Figure 4 displays an example of a projectile. The projectile requires tolerances of less than one thousandth of an inch on the outer diameter, and the front face. Only in this manner can a properly aligned impact condition be achieved. The high pressure gas expands as the projectile is accelerated down the barrel and the desired velocity is achieved before impact occurs. Before every shot, the barrel and breech are cleaned using ethyl alcohol on a large swab to remove any residues.

Figure 4. Example of a Projectile

In order to ensure that the experiment is successful, many systems must be specifically tuned. The first system is the barrel and breech alignment. Thirteen adjustable screws suspend these pieces of hardware. Nine fix the position of the barrel in three barrel holders each containing three adjustable screws in 120 degree angle increments. Four supports—two on each side—hold the breech in its desired location. These components are displayed in Figure 5.

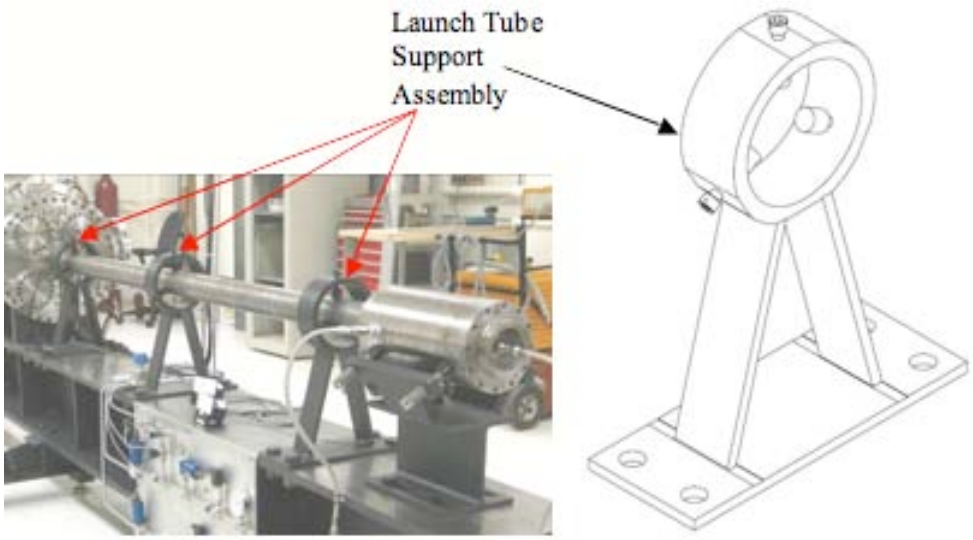

Figure 5. Barrel and Breech supports

In order to ensure the barrel and breech are properly aligned, a class 3b He:Ne laser is retro-reflected down the entire length of the barrel and back. The thirteen different adjustable screws are adjusted until the reflected spot is less than a centimeter away from the point of origin—this indicates an alignment of about 1 mrad. To ensure very flat impact conditions, tilts of 1 to 2 mrad or less are desired.

Now that the firing components of the gun itself are prepared, the catching—or momentum stopping—components must be ready to absorb energy from the impact and associated shrapnel. Within the catch tank portion of the gun, several layers of energy absorbing materials are employed. The catch tank is about two feet in diameter made of mild steel about half an inch thick. At the very rear of the catch tank, there is a blast shield—an extra layer of mild steel to prevent any debris from striking the rear surface of the catch tank. In front of this, sheets of honeycomb aluminum are placed. These sheets serve as energy absorbers, and the number required per shot and survival rate depend on the momentum of the bullet. Visual inspection can clearly deduce when the sheets are spent. In front of this, there is a sliding baffle to absorb energy. The baffle has nylon wheels and is a sealed cylinder of steel. Next, there is more of the honeycomb aluminum. Lastly, there is a plate of aluminum which is the first catch tank element impacted by the projectile. When impacted, this plate compresses the honeycomb material relatively uniformly causing energy to be dissipated. All together, the catch tank in its firing ready state is displayed in the cut away in Figure 6.

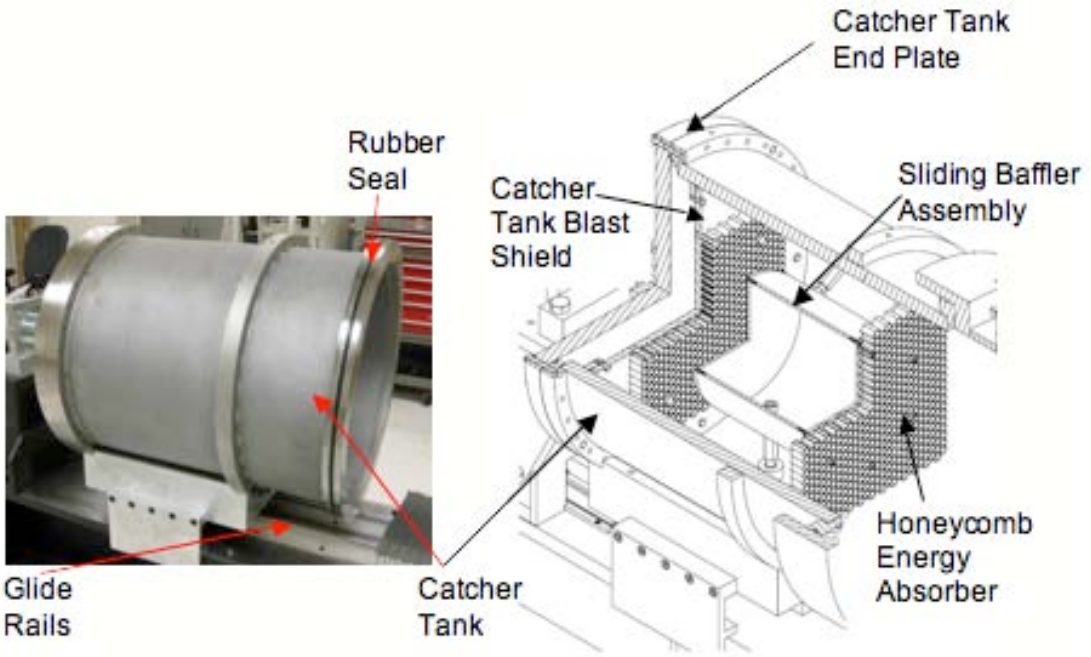

Figure 6. Catch tank assembly

2. Improving Gas Gun Performance

Since the single stage gas gun used in this research is new to the NPS, a portion of this work is spent optimizing the performance of the system. In the work of Ho [8], the gun was assembled and preliminary shots fired. These results showed that the gun was operational and producing well characterized impacts. This research is the first use of this gun facility to actually collect data. This requires us to routinely refine and measure projectile velocity and tilt, and use the velocity interferometer diagnostic system. This will be described in more detail below. Since this gun was built with the same design as a Sandia National Labs gun, the performance of the NPS gun should be similar to that of the Sandia gun. Actual performance must be measured to verify this similarity. Figure 7 displays shots recorded by Sandia in blue and shots recorded by NPS prior to the beginning of this research in pink. The NPS shots fall within the scatter of SNL's performance curve.

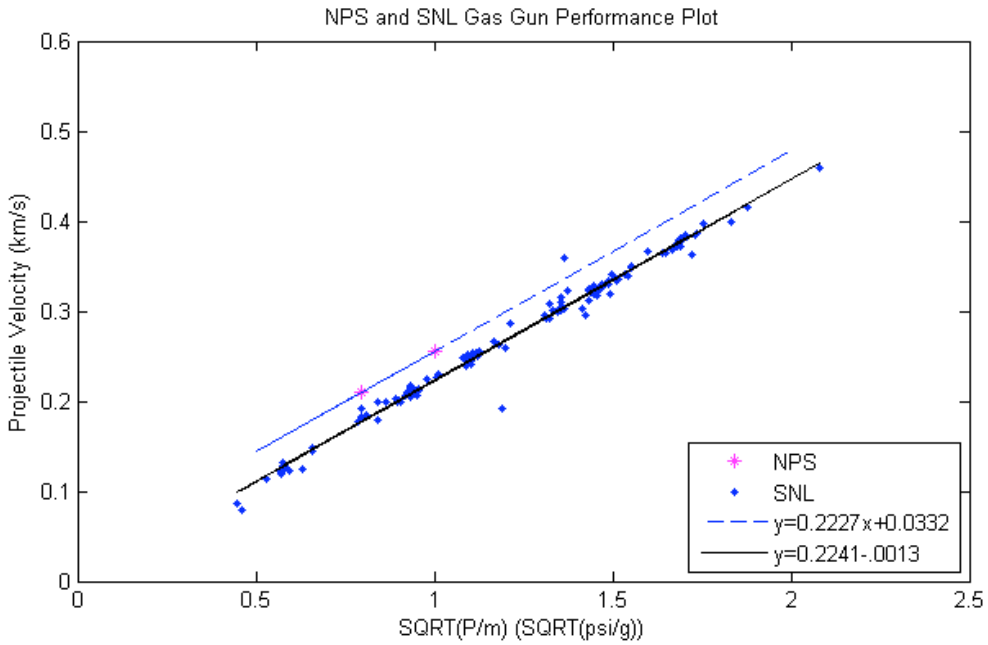

Figure 7. Combined data from shots of 76mm bore gun (From [8])

The horizontal axis is the square root of the ratio of the projectile's mass to the pressure of the breech when fired. The vertical axis represents the measured projectile velocity. One of the goals of this research is to characterize deviations from the Sandia performance curve. Incorporation of a few system modifications to the NPS gun will allow a better performance curve to be obtained. This will allow us to better predict gun performance. We will describe these improvements.

3. Other Gun Improvements

Simple improvements were made to the gun system to enable more efficient experiments.

a. Pressure Gauge

The originally installed pressure gauge for the breech charge pressure was an analog gauge that had a maximum reading of 4000 psi. Since the breech is only rated at 2000psi, the maximum safe charge pressure is set at 1200 psi. For most shots performed in this work, the operational charge pressure was between 200 and 400 psi. Making readings at this level 10% accurate or less on the analog gauge; this leads to large

uncertainties in the determination of performance. To improve this situation, a digital gauge with a read out range of 0-3000 psi with an accuracy of ± 1 psi was installed. This gauge dramatically improved the reliability of breech pressure measurements. In addition, a second digital pressure readout was installed in the control panel so that breech pressure could be read immediately before firing the gun. There is still room for improvement in this system, as the thermocouple is still relatively low resolution. Another thermocouple should be acquired to match the new gauge's sensitivity. Use of the new breech pressure measurement system has brought our performance points closer to those measured by Sandia.

b. Scale for Bullet Mass

Initially, the only scale available for acquiring the mass of the projectile and impactor was accurate to only ± 1 gram. At first, this did not seem to be limiting to the accuracy of the performance curve based on masses on the order of 350 grams. However, for little cost, a more sensitive scale was acquired with an accuracy of ± 0.1 gram. This increase in precision will help improve the accuracy of the gun performance curve.

C. SAMPLE CHARACTERIZATION

In order to make accurate dynamic property measurements, we must first characterize certain initial properties for our ceramic material. This initial characterization is important to establish the baseline properties that are needed to interpret the dynamic properties we intend to measure. This is especially important for sintered materials like polycrystalline ceramics to be sure this material is close to isotropic. Previous experimental results of Gust and Royce [10] on similar materials have clearly shown that initial sound speed depends strongly upon initial density, so that even small deviations in initial density cause measurable difference in initial sound speed and dynamic properties. Figure 8 displays these differences graphically.

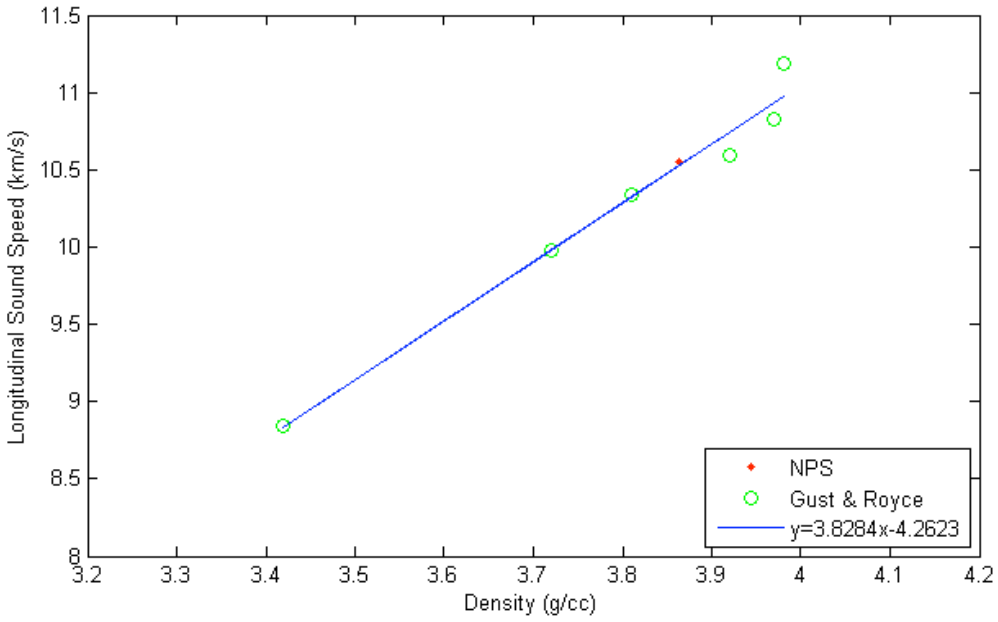

Figure 8. Comparison of longitudinal sound speed for various density ceramics

The horizontal axis is density in grams per centimeter cubed, and the vertical axis is longitudinal sound speed in kilometers per second. There appears to approximately be a linear relationship between the two. The measured values at NPS fit in nicely with the previous work of Gust and Royce [10], as shown in Figure 8 with a red square. Shock properties, such as the Hugoniot and the dynamic yield strength, are also expected to depend upon initial density. For this reason, we had immersion density measurements done at Los Alamos National Laboratory and performed ultrasonic measurements of sound speed in our laboratory.

1. Initial Density

Initial density was measured at Los Alamos National Laboratory (LANL) using a standard immersion technique, which is based on Archimedes principle. This idea is to measure the weight of the sample both dry and submerged in water, and use the difference to find density. The LANL value was ρ_0=3.864 ± 0.005 g/cc. This is to be compared with other similar polycrystalline alumina-based ceramics, and to the value for single crystal Al_2O_3 (sapphire; ρ_0=3.985 g/cc).

2. Elastic Sound Speeds

Sound speed is a very sensitive indicator of a material's elastic properties and is usually easy to measure accurately for solid materials. We used a commercially available ultrasonic pulse-echo system made by Panametrics Inc. (a division of Olympus). This system consists of a pulsar unit connected to either a longitudinal or shear transducer, with a digital oscilloscope used to observe pulses and measure timing between them as prescribed by Olympus [9]. Two thicknesses of ceramic (approximately 3 and 6 mm thick) were measured and results repeated essentially exactly. This gives us confidence that our samples are of uniform quality. Representative results for sound velocity are shown in Table 1 along with density and literature values for similar materials.

Table 1. Initial properties for Corbit-98 ceramic and similar Al_2O_3 polycrystalline materials

Material	Initial density (g/cc)	Longitudinal Sound Speed C_L (km/s)	Shear sound speed C_S (km/s)
Corbit 98	3.864	10.55	6.18
AD-85 [10]	3.42	8.84	5.06
P-3142-1 [10]	3.72	9.98	5.88
Al-995 [10]	3.81	10.34	6.21
AD-995 [11]	3.89	10.56	6.24
Hot pressed [10]	3.92	10.59	6.17
Lucalox [10]	3.97	10.83	6.38
Single crystal, Z-direction	3.985	11.19	N/A

Our material compares very favorably with hot-pressed ceramic as described by Gust and Royce [10], and the Coors AD-995 material measured by Grady [11] and Reinhart [12]. From the measured properties, many other elastic properties may be

calculated. Specifically, once we have values for initial density, longitudinal sound speed (C_L) and shear sound speed (C_S), we can find other relevant elastic properties:

$$C_B = \sqrt{C_L^2 - \frac{4}{3}C_S^2}\ ;$$

$$F = \rho_0 C_L^2\ ;$$

$$G = \rho_0 C_S^2\ ;$$

$$K = \rho_0 C_B^2\ ;$$

$$\nu = \frac{(3K - F)}{(3K + F)} = \frac{(F - 2G)}{2(F - G)} = \frac{(3K - 2G)}{2(3K + G)};$$

Table 2. Calculated properties for Corbit-98 ceramic and similar Al_2O_3 polycrystalline materials

Material	Bulk Sound Speed (C_B) (km/s)	Longitudinal Modulus (F) (GPa)	Shear Modulus (G) (GPa)	Bulk Modulus (K) (GPa)	Poisson Ratio (ν)
Corbit 98	7.77	430.	147	233	0.239
AD-85 [10]	6.63	267	87.6	151	0.256
P-3142-1 [10]	7.31	371	129	199	0.234
Al-995 [10]	7.45	407	147	211	0.218
AD-995 [11]	7.72	434	152	232	0.232
Hot pressed [10]	7.84	440.	149	241	0.243
Lucalox [10]	7.94	466	162	250	0.234
Single crystal, Z-direction	N/A	499	N/A	N/A	N/A

D. HUGONIOT MEASUREMENT EXPERIMENTS

1. Shock Compression Experimental Techniques

Our research goal was to do very fundamental characterization of the response of this ceramic to shock wave compression. Specifically, we wished to determine the dynamic yield strength (HEL), the shock Hugoniot, and the dynamic strength in tension (spall strength). To do this, we use well-developed shock compression experimental techniques. For any material, the most fundamental description of its shock properties is the shock 'Hugoniot'. This is the locus of end states that are obtained through the shock compression process. Typically two parameters are measured: shock and particle velocity. This is done to be able to satisfy the governing equations and thus be able to calculate other shock properties such as pressure and density. The governing equations are called the jump conditions, and are typically expressed as:

Mass: $$\frac{\rho_0}{\rho} = 1 - \frac{u_P}{u_S}$$

Momentum: $$P - P_0 = \rho_0 U_S u_P$$

Energy: $$E - E_0 = \frac{1}{2}(P + P_0)(V_0 - V)$$

It is easy to see that this is a set of three equations in five unknowns, and that measuring U_s and u_p allows solution. The first goal, therefore, was to measure shock and particle velocity over the range of impact conditions possible on the gas launcher.

2. Hugoniot Measurements

To do this, we use well-developed experimental techniques. First, the flyer velocity is measured using electrical shorting pins as described in the work of Ho [8], or is inferred from the performance curve. We also must measure the shock transit time in the target to be able to use its known thickness to determine U_s. We do this as shown in Figure 9.

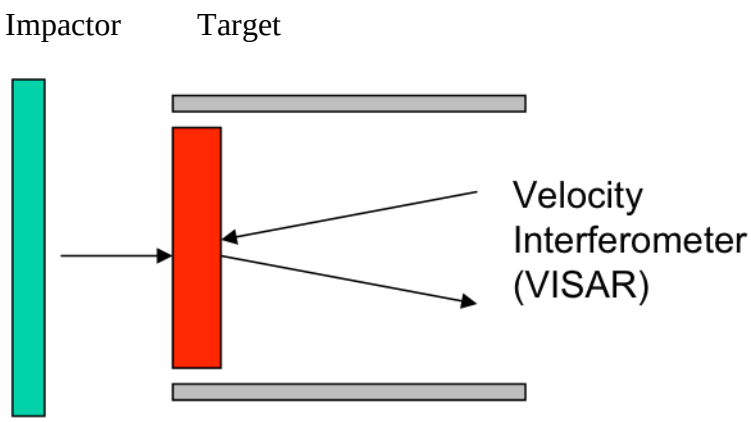

Figure 9. Sketch of parallel plate impact

In order to measure the very short times required for shock waves to travel through a the ceramic target (on the order of a microsecond), times must be resolved down to nanoseconds. Shock transit times can be obtained from piezoelectric (PZT) pins or from multiple velocity interferometers, or from a combination of these. As shown in Figure 9, we have chosen to use PZT pins to record the impact time, including the correction for impactor tilt, and use a velocity interferometer to detect shock arrival at the back side of the sample. The preferred velocity interferometer for shock wave research is called the Velocity Interferometer System for Any Reflector (VISAR). The principles defining the use and calibration are described in detail by Hemsing in 1978 [13]. Some materials are reflective enough to allow direct interface with the VISAR light, but this is not the case for our ceramic. For less reflective materials, such as ceramics, a very thin foil may be applied to the VISAR side of the target to increase reflectivity. The simplest experiment of this kind is a free surface experiment. However, a potential drawback to the free surface experiment is that the free surface causes a complete release wave to be reflected back into the sample, causing the interface being observed to be at zero pressure. This in turn does not allow quasi in-situ wave profile data to be obtained. To allow quasi-in-situ particle velocity measurements, another kind of experimental geometry can be used. This experimental setup uses a thin, reflective foil mounted to the

target with a thick window behind it. The window serves to prevent full release during the first wave interaction at the back surface of the sample. Figure 10 shows the geometry for this method.

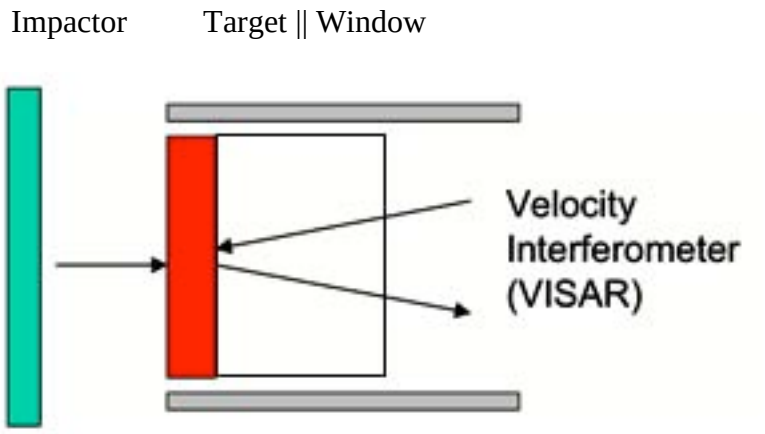

Figure 10. Sketch of parallel plate impact with foil and window

VISAR data is recorded on a fast digital oscilloscope (Tektronix model DPO4104), and an analysis code is used to convert the raw data into a time-resolved wave profile of particle velocity at the interface between Corbit ceramic and the z-cut single crystal sapphire window. A sapphire window was chosen because it is a very close shock impedance match to the ceramic, and allows interface reflections to be minimized. For measurement of shock velocity, we only use the arrival time of shock wave, but we will discuss further uses for this data.

To measure shock velocity, the time from impact until the breakout of the first wave must be precisely known, as must the thickness of the target. The ratio of target thickness to arrival time of the first data is the shock speed.

$$U_s = \frac{x}{t}$$

For very low amplitude stress in elastic compression, the calculated wave speed must be close to the longitudinal sound speed. But for finite amplitude waves, some shock-up will be observed, and we expect to measured shock velocities that are greater

than the value of C_l. To determine the particle velocity, we use the known properties of the impactor material and our measured shock velocity and impedance matching techniques. This is described in Figure 11.

We wish to find u_{P2} in the target and get a point on the $U_S - u_P$ curve for the target. We do this by using the fact that across the impact interface, pressure and particle velocity must be conserved as shown in Figure 11.

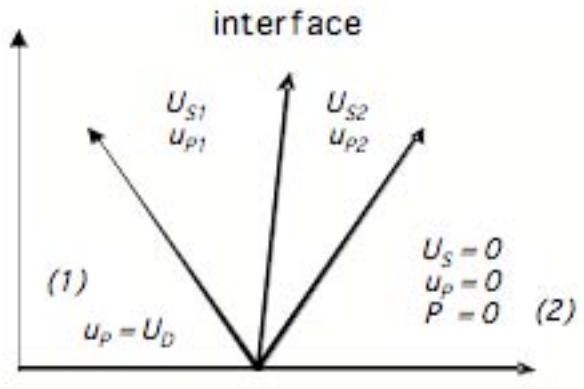

Figure 11. Impact details for impedance matching technique

Note, that for the flyer (material 1) in general, we know its Hugoniot, and so we have:

$$U_{S1} = S_1 u_{P1} + C_1$$
$$\Rightarrow P_1 = \rho_{01}(S_1 u_{P1} + C_1) u_{P1}$$

But, we also know that: $u_{P1} = U_D - u_{P2}$.

So, we can write: $P_1 = \rho_{01}(S_1(U_D - u_{P2}) + C_1)(U_D - u_{P2})$. This can be multiplied out and expanded:

$$P_1 = \rho_{01} S_1 U_D^2 - 2\rho_{01} S_1 U_D u_{P2} + \rho_{01} S_1 u_{P2}^2 + \rho_{01} C_1 U_D - \rho_{01} C_1 u_{P2}$$
$$P_1 = (\rho_{01} S_1) u_{P2}^2 - (2\rho_{01} S_1 U_D + \rho_{01} C_1) u_{P2} + \rho_{01}(S_1 U_D^2 + C_1 U_D)$$

Since U_s in the target is measured, the pressure in the target, P_2 can be found:

$$P_2 = \rho_0 U_S u_{P2}$$

where we wish to find u_{P2}. Pressure in impactor and target are equated:

$$(\rho_{01}S_1)u_{P2}^2 - (2\rho_{01}S_1U_D + \rho_{01}C_1)u_{P2} + \rho_{01}(S_1U_D^2 + C_1U_D) = \rho_0U_Su_{P2}$$

Subtracting yields:

$$(\rho_{01}S_1)u_{P2}^2 - (2\rho_{01}S_1U_D + \rho_{01}C_1 + \rho_0U_S)u_{P2} + \rho_{01}(S_1U_D^2 + C_1U_D) = 0$$

This is a quadratic equation, and we can find the roots and so the value of u_{p2}.

If the flyer and target are the same, this is called symmetric impact, and the analysis becomes even simpler. This analysis gives us a way to calculate the particle velocity behind the shock wave that is moving to the right in our sample. When combined with U_s in the target, we now have the first point on the curve that describes the locus of end states achievable in a single shock; this is called the shock Hugoniot. Ceramic materials have ultrasonic wave speeds that strongly depend upon their initial density. We see this in Table 1. We also expect the shock Hugoniot to also be sensitive to initial density. For this reason, initial characterization must be meticulously done. We note this because there is a relatively large scatter in literature shock properties of alumina-based ceramic materials. At least some of this scatter may be due to differences in starting material.

Shown in Figure 12 are some data from the literature for alumina-based ceramics all at about the same initial density, but with some small variations. This clearly shows that results can show scatter. This is not the case for other kinds of materials that are full density. For example, metal Hugoniots from various sources typically show very good agreement.

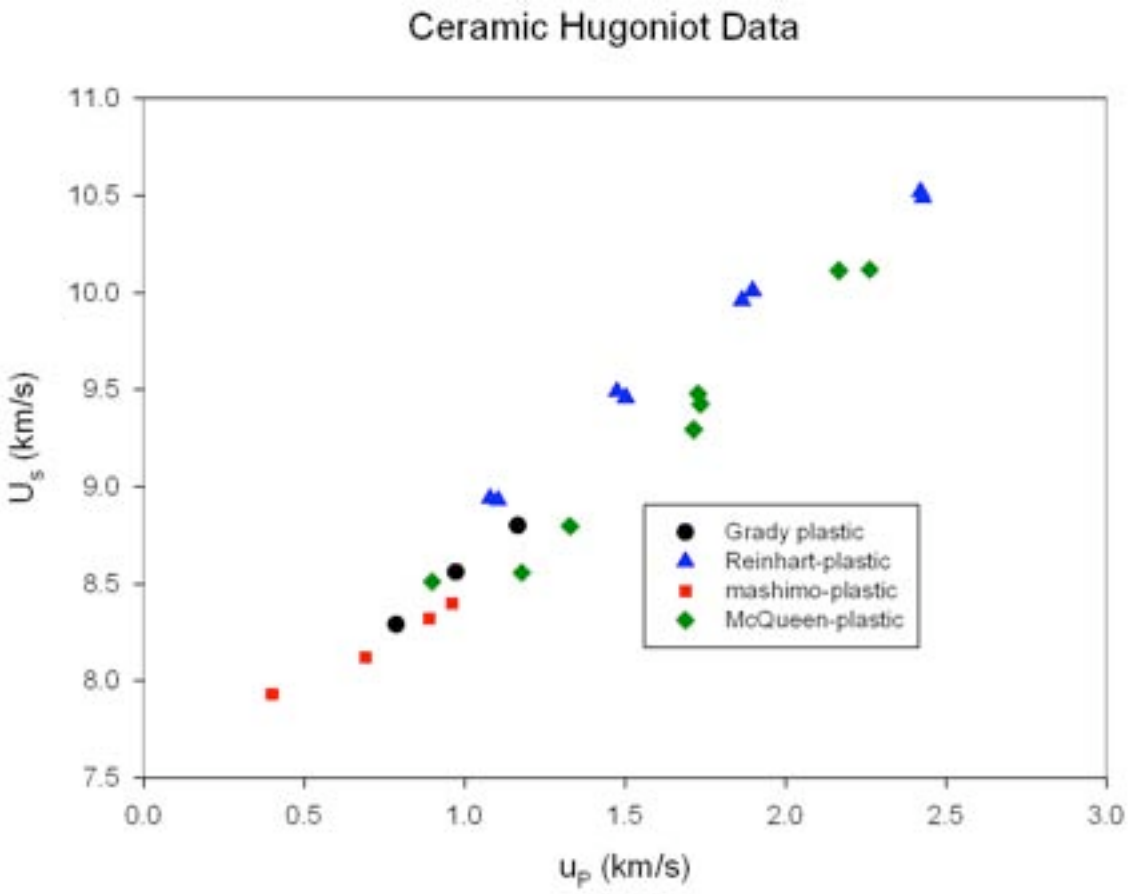

Figure 12. Ceramic data from the literature shows relatively large scatter (After [11, 12, 14, 15]).

Ceramic materials, as for all solids, will first respond elastically when shock compressed, but will then respond plastically. The NPS gas gun is not able to go significantly above the dynamic yield point for Corbit-98 ceramic, and so measurements here are done for elastic compressions. A small number of experiments at higher stress were done at Los Alamos National Laboratory. One goal of this research is to establish the elastic Hugoniot for this material as well as is possible. Results are shown in Figure 13.

E. STRENGTH MEASUREMENTS

Another goal of this research was to determine the dynamic yield point for the ceramic studied. This is called the Hugoniot elastic limit. At this point, there is a cusp in the shock Hugoniot in P-V space, as shown in Figure 13.

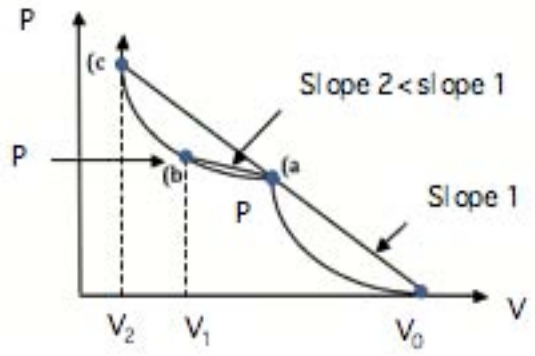

Figure 13. Shock Hugoniot for a material with strength

We will be doing shock experiments both above and below the dynamic yielding point labeled '(a'. Experiments done above the yield point can be used to actually measure it. This is an important input point for simulations involving this material. State (a) in Figure 13 is called the Hugoniot elastic limit and is called σ_{HEL}. In order to measure this stress, it is necessary to shock to a stress state that is higher. As seen in Figure 13, this will then cause two shock waves to be generated. One takes the material to state (a) and the other to the final stress state, state (b) for example. The VISAR system is then used to observe these waves, and by measuring the state at the top of the first wave σ_{HEL} can be calculated. In detail, this calculation depends upon experimental details, such as if a window was used. We will show results from these measurements below.

F. SPALL MEASUREMENTS

Another goal for this research was to measure the spall strength of Corbit-98. The spall strength is equivalent to the dynamic strength in tension. For a brittle material like ceramic, we expect the spall strength to be much smaller than the HEL. In practice, the spall strength is calculated from a free surface wave profile obtained from an experiment

that is designed to let two release waves interact in the target and put the material into tension dynamically. This is done by choosing impactor and target thickness to be just right to let the reflected wave from the target free surface to reach the center of the sample at the same time as a release that originates from the back surface of the impactor. This is shown in Figure 14 in distance-time (x-t) space.

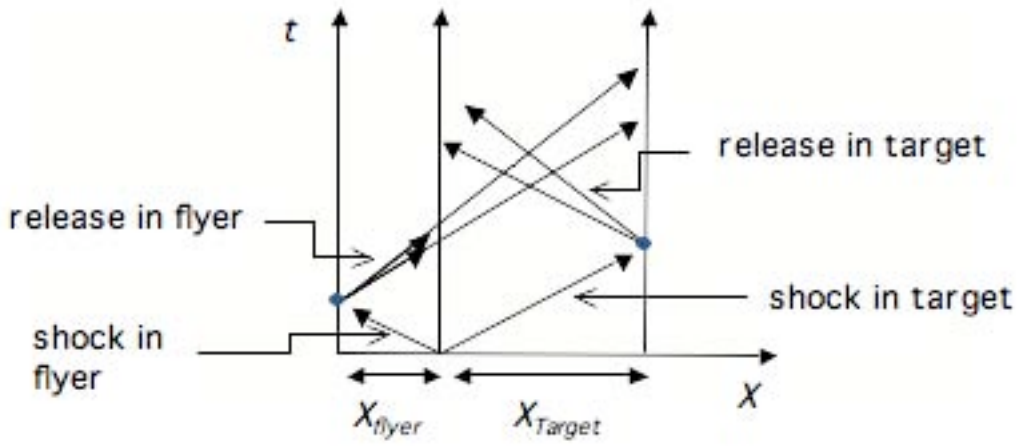

Figure 14. Wave interactions leading to spall

After impact, two shock waves are created, one moving to the right in the target, and one moving to the left in the sample. The shock in the target will reflect from the right surface of the target as a full release because this is a free surface. This reflected release is shown as a fan moving to the left in the target. Similarly, the shock moving to the left in the flyer reaches the left surface, which is supported by a foam material. A deep release wave is then reflected to the right and is shown also as a fan. These two fans have particle velocity vectors that point in opposite directions, causing tension in the sample. Information about tension is carried to the right surface of the target by waves and detected with the velocity interferometer.

An example of the kind of data recorded for this kind of experiment is shown in Figure 15 using a wave profile from a calibration shot.

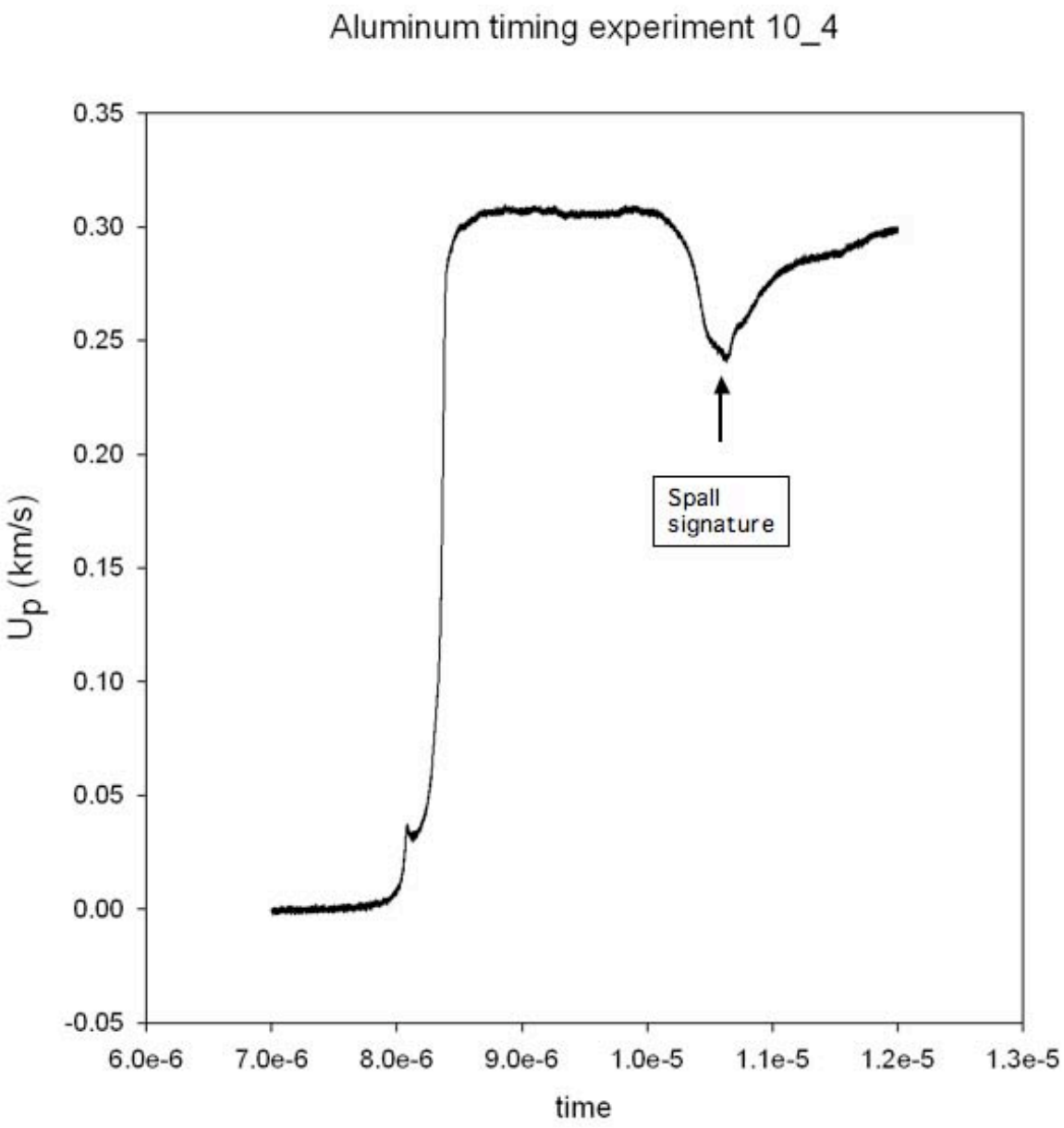

Figure 15. Annotated AL6061 wave profile from shot 10_4

The formula to calculate spall strength is:

$$P_{spall} = \rho_0 C \Delta u_{FS}$$

Where ρ_0 is initial density, C is the wave speed, and Δu_{FS} is the difference in particle speed from the maximum u_{FS} at shock state (labeled as 1 on wave profile), and the minimum immediately after (labeled as 2 on wave profile). The wave speed used in

simple materials is the bulk sound speed for ductile materials. For brittle materials, we cannot precisely determine the spall strength from use of bulk sound speed as the wave speed in this calculation. However, for simplification, we knowingly use it to acquire an approximate value of spall strength.

G. MATERIAL CHARACTERISTICS

Using pulse-echo sound velocity measurement techniques, as described in Olympus [9], shear and longitudinal sound speeds in AL6061, sapphire impactors and sapphire windows were measured. The results of these measurements are shown in Table 3. Our results for aluminum are in good agreement with those given in Marsh [15].

Table 3. Measured sound speeds for aluminum and sapphire

Material	C_L Measured (km/s)	C_L Actual [15] (km/s)	C_S Measured (km/s)	C_S Actual [15] (km/s)
AL6061	6.31	6.400	3.176	3.150
Sapphire Impactor	11.38	11.19	N/A	N/A
Sapphire Window	11.23	11.19	N/A	N/A

The process of acquiring the sound speeds uses a 12.5 GHz oscilloscope from Tektronix (DPO 71254), as shown in Figure 16.

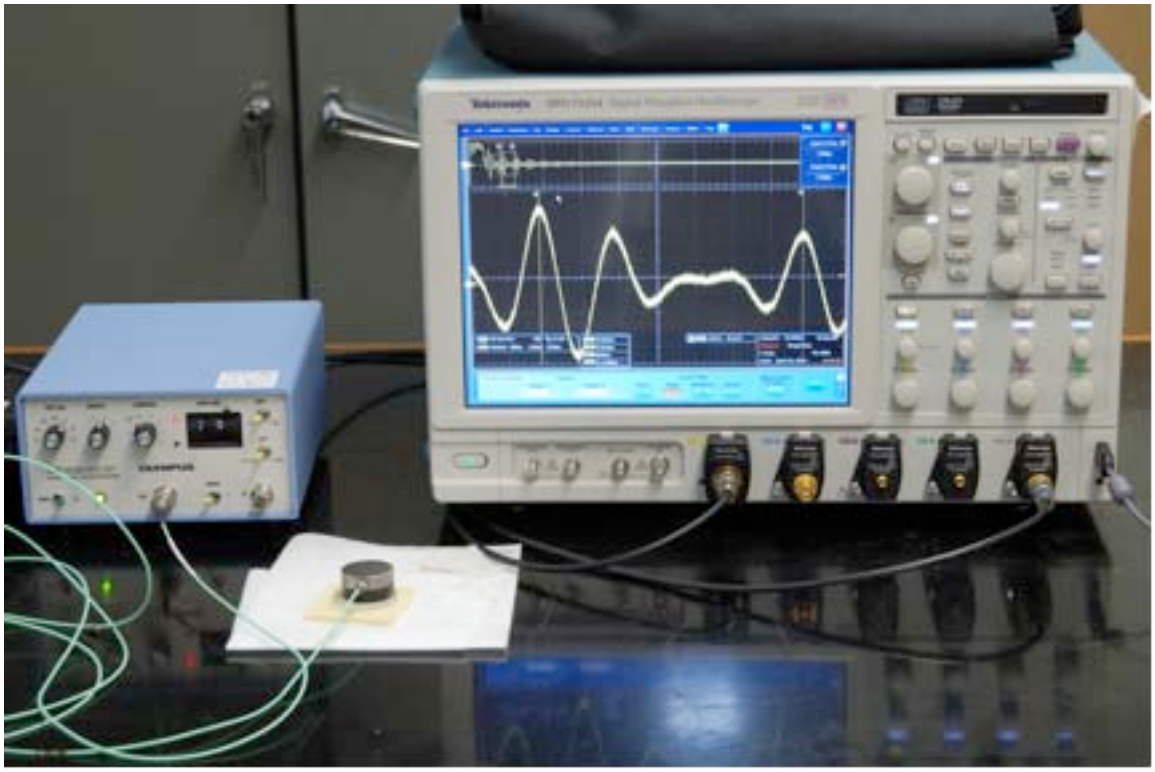

Figure 16. Example of measuring pulse echoes for sound speed measurements

H. TARGET DETAILS

1. Target Plate

The simplest design for a target plate is a single homogenous material in a six-inch diameter disc with three holes for mounting. Examples of these are shown in Figure 17. In his thesis, Ho describes using such targets in preliminary assembly and calibration of the gun [8].

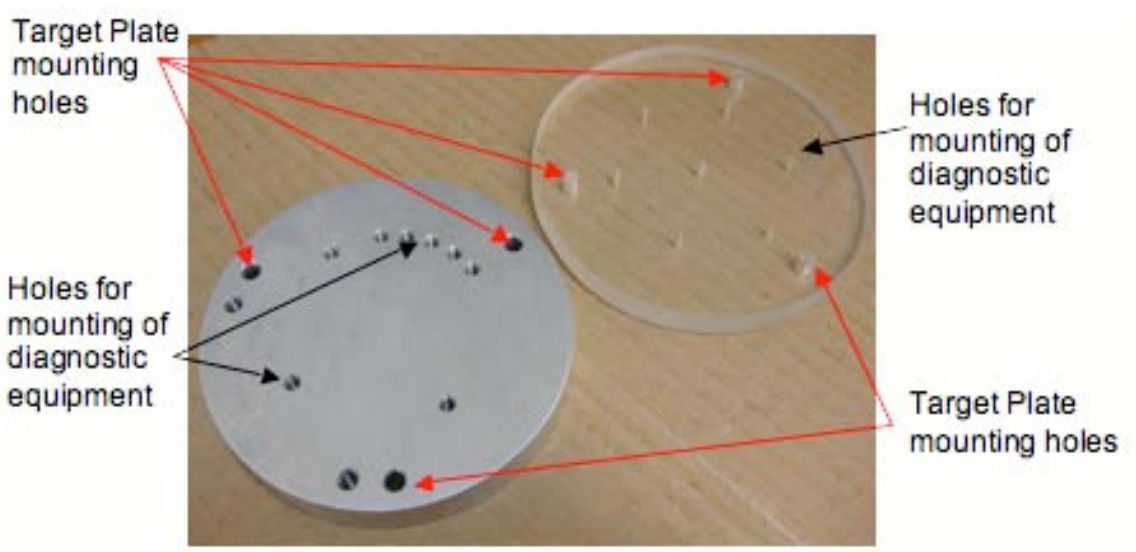

Figure 17. Examples of Target Plates

For our ceramic experiments, which use both VISAR and velocity pin diagnostics, a more complicated design was required. Specifically, the target plate (made from aluminum 6061) must have a total of fifteen holes to accept various pins, and be machined to a tight tolerance for flatness. The as-received plate is lapped flat using a fine sand paper on a granite flat to better than 0.012mm (12 microns). Similarly, the impact surface of the projectile must be lapped to be flat to 0.012 mm and normal to the axis. An example of this lapping process being performed on a bullet is shown in Figure 18.

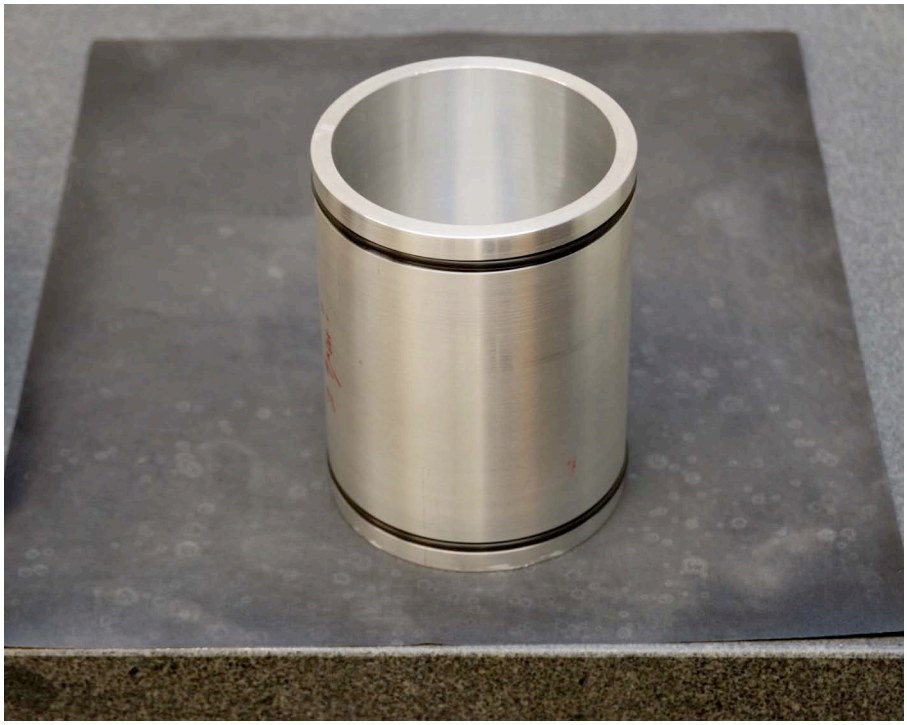

Figure 18. Projectile being lapped on a 600 grit sand paper on top of a granite flat

Figure 19 shows a drawing of the target holding plate with all of its holes. From outer radius towards the inner radius, the three outer most holes are used for mounting the target plate to the gun target mounting plate, which is normal to the barrel axis. The next smaller radius hole is used to mount the VISAR laser probe holder in its specific location. Subsequently, seven holes are required for six velocity shorting pins and a single ground pin. In addition, three piezoelectric impact pins take up three slightly larger than the velocity pin holes. Lastly, the ceramic sample itself occupies the largest hole in the center of the target plate.

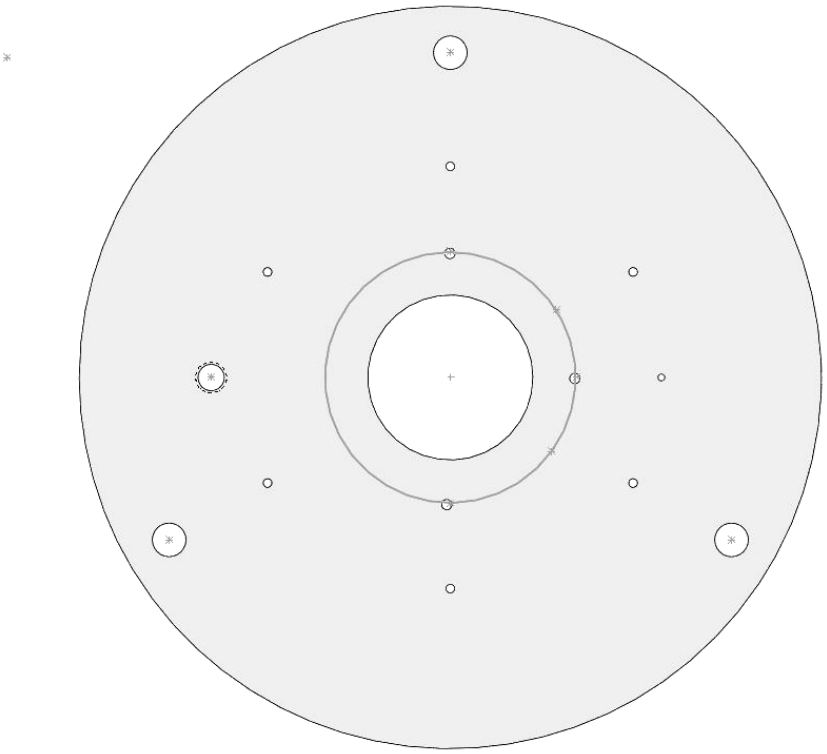

Figure 19. Schematic of Target plate

2. VISAR Details

The principal diagnostic for the research described here was a velocity interferometer as mentioned above. It is called a VISAR, and has been used to diagnose shock compression experiments for many years. Our VISAR system was acquired from National Security Technologies (NSTEC), and represents the state-of-the-art for such instruments. This system benefits from a small physical footprint and extreme user-friendliness. This makes it perfect for research done by students at the NPS. But, the actual VISAR cavity is only one component of the overall system. Another part of the system is a class 4 doubled frequency Nd:YAG solid state continuous wave (CW) laser. This laser was procured from Coherent, and is set up to operate in the green at 532nm wavelength. For safety and convenience during test preparations, the laser output is

embedded in an optical-fiber system that serves to contain the light and prevent accidental exposure. The output of the laser is focused into a 50 μm step index optical fiber through a pockels cell. This fiber goes to the gun's experimental chamber where it is coupled to an optical fiber probe that goes through a vacuum flange and into the gun experimental chamber. Light is focused onto the target by a plano-convex lens. Reflected light is collected by the same lens and sent back to the VISAR by another optical fiber. Light signals from the interferometer cavity are routed to four 928 photomultipliers, and their electrical signals are sent to a Tektronix DPO4104 transient recorder. After the experiment this data is collected on a computer for analysis. Example of this data will be given below.

3. Velocity Pins

A stepped circular array of electrical shorting pins is used to measure tilt and impact speed. Each of the seven pins is placed a different height. Six of the pins are arranged at 60 degrees from each other about a common diameter circle. The ground pin is the first to be hit, but may be placed at any position on the circle. The pins are wrapped in heat shrink insulation in order to be isolated electrically until struck by the projectile. Note that the pins short across the projectile through the ground pin. The non-impact sides of the pins are individually wired to a harness that converts simple wire to a coaxial cable with BNC connector. These cables then go to a pin-circuit, which generates an electrical pulse for each pin that is shorted. By doing a least-squares fit to the pin times at the various lengths and angles, both projectile velocity and tilt can be measured; this is done in an analysis computer program. By comparison of the rate of impact and the angular location of the pins, the tilt is measured.

4. Piezoelectric Pins

Piezoelectric (PZT) pins are used for two purposes. First two pins are set flush with the impact surface of the target plate and opposite each other to allow measurement of impact time. Secondly, one pin is set so that its active end is in front of the impact surface of the target plate to allow all electronics to be triggered before impact occurs. In both cases, the PZT pins are attached directly to electronic equipment using 50 Ω coaxial

cable. So to summarize, two of the pins are flush with the surface of the target so that the moment of impact is known precisely, and the third pin is used to trigger both the LASER and data recording instrumentation.

5. Sample Details

A hole is machined in the center of the target plate that is slightly larger than the outside diameter of the ceramic sample. The sample is inserted and held in place with glue. The ceramic manufacturer supplied ceramic squares 50 mm by 50 mm. In order to fit in the round target plate hole, the ceramic was cut using a diamond hole saw. This process is delicate, deliberate and time consuming. Because ceramic is a super-hard material, only a diamond tipped or diamond imbedded blade can cut it. Even using such tools, the cutting must be done slowly to avoid cracking the brittle material. Also, due to the immense heat tolerance of ceramic the sample must be immersed in a coolant fluid to prevent extreme temperatures.

Once the ceramic disc is cut, it is lapped using a diamond impregnated lapping plate followed by polishing with fine grit alumina slurry and a rotating wheel. The lapping plate comes from UHL Technologies, and is designated DIABLAP. An example of a sample being lapped is in Figure 20:

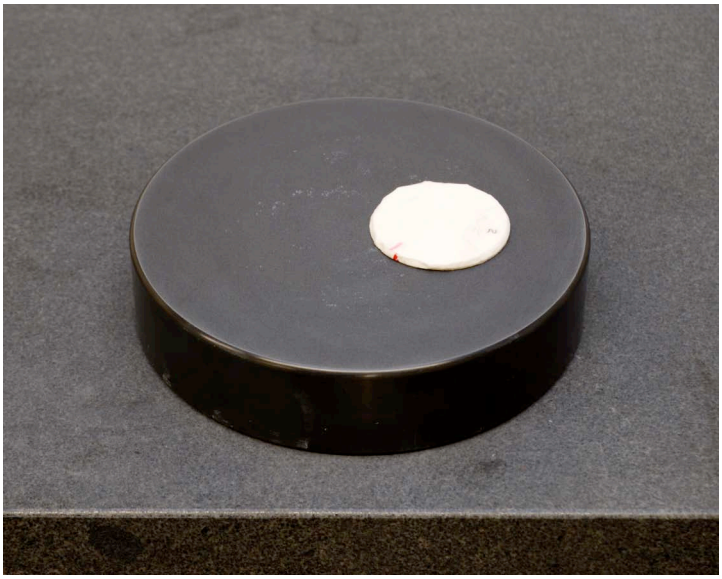

Figure 20. Lapping plate with ceramic sample on top

Ensured of its flatness for proper impact, a thin sheet of reflective foil—such as stainless steel shim less than 20 μm in thickness—is glued in place between a sapphire window and the ceramic as previously described. Later experiments used a vapor deposited layer of aluminum on the window surface. This reflective layer is used to provide reflected light from the sample/window interface to return to the VISAR system for measurement.

Once completed, the target plate is mounted and the projectile is placed in the breech, both the breech and the catch tank are sealed and made ready for evacuation. Once the system is sealed, the vacuum system is turned on and brought down to less than 30 mtorr as previously described. The vacuum system linked to the gun assembly is pictured in Figure 21. Having fired the shot, data is successfully acquired, and results can then be saved for analysis.

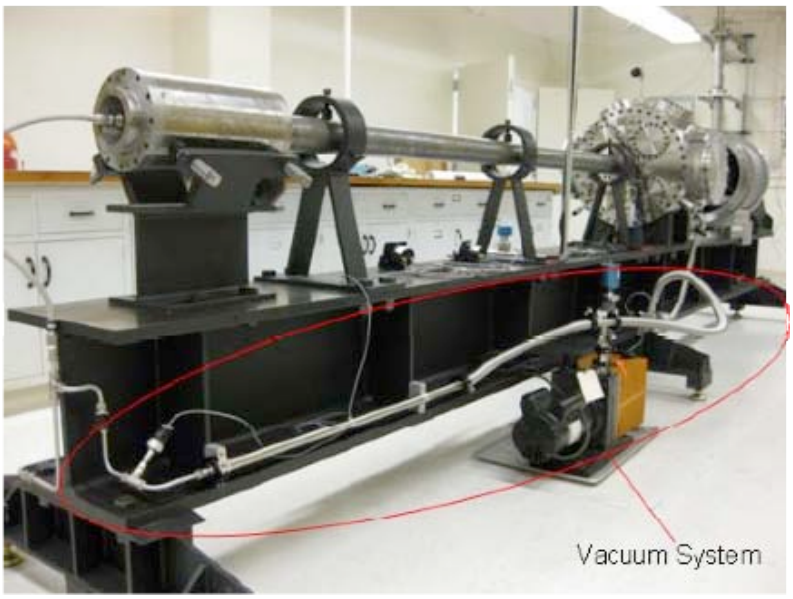

Figure 21. Vacuum System

THIS PAGE INTENTIONALLY LEFT BLANK

III. EXPERIMENTAL RESULTS

In this section, we will discuss the results of our experiments. Data will be shown along with appropriate analysis. The techniques described above were used for experiments at the NPS and at Los Alamos National Laboratory (LANL). Experiments to higher stress level were possible at LANL using a higher performance gas gun. As we will show, results from the two laboratories are very complementary. Full page views of wave profiles are included in the appendix.

A. ALUMINUM SHOTS

To begin this research, our instrumentation system had to be calibrated using a well-studied material for system response and for system timing. For this reason, experiments using aluminum alloy 6061 in symmetric impact configurations were performed. *These were the first experiments that used the VISAR and PZT pin diagnostics done in this laboratory.* For this reason, we expected to make system changes to fine tune the instrumentation. We chose 6061-T6 aluminum as the material used for the first two experiments, because it has been widely used in shock experiments, and much is known about its dynamic response. More importantly, these experiments also allowed us to determine the difference in timing between the electrical (PZT) pins used to determine impact time, and the optical/electrical VISAR signal used to find shock breakout time.

1. Timing for Instrumentation

a. Shot 10_1

The first shot done, designated shot 10-1, was a symmetric impact shot designed to test the VISAR system. The desired impact velocity was 0.2 km/s. The projectile used weighed 372 grams. Target density was taken to be 2.703 g/cc. The three inch gun in Room 027 of Spanagel Hall at NPS was used to throw an aluminum projectile at an aluminum target plate. Using the gas breech performance curve, the necessary pressure to achieve this speed is between 285-315 psi. The anticipated particle speed in

the target was 0.1 km/s, as predicted from elementary shock physics, because the projectile and target were both made from 6061 aluminum. Similarly, since this was a free surface shot, the velocity measured with the VISAR should be twice the particle velocity and very close to the same as the projectile velocity.

The shot was very successful, with the exception of one flush pin malfunctioning. This malfunction is believed to be caused by the cable loosening prior to the shot. As a result of this, we now solder the cable to the pins before installing the target in the gun. Since the Hugoniot equation of state is known for Al6061, the time of impact can be determined from the known transit time through the sample, and the thickness of the target. The wave profile, as measured for this shot, is included in Appendix and is of very high quality. Tilt and projectile velocity were not measured with velocity pins for this shot to reduce complexity, and because the focus of the experiment was to demonstrate that the VISAR system worked. Projectile velocity was inferred from the gun performance curve and from the measured wave profile. This experiment was pivotal in demonstrating that the VISAR system was functional. A free surface velocity of 0.22 km/s was obtained with the VISAR, comparing well with the velocity expected from gun performance of 0.20 km/s. Because one flush pin failed, we could not determine an accurate system timing correction. This meant that another calibration shot was needed.

b. Shot 10_4

The second shot on 6061 aluminum was performed to test data collection systems and find a correction time between VISAR and PZT pins. The front of the projectile was lapped true and served as the impactor. Measured projectile velocity was 0.308 km/s, using the VISAR determined free surface velocity. Impact stress was calculated to be 2.29 GPa. Four flush PZT pins were used to find projectile tilt, which was determined to be 0.71 mrad. The target plate thickness was measured to be 6.479 mm. A detailed comparison of the electrical signal delays and the optical signal delays from this data were made using the measured longitudinal sound speed—6.479 km/s and measured shear velocity of 3.176 km/s. Both of these values for sound speeds are typical

for AL6061. We took the fast rise in the elastic wave as the arrival time and based on this, we found the correction to be to add 20 ns to the measured time difference between the average of the flush pins and the VISAR measure arrival of the elastic wave. The expected uncertainty from the flush pin time is equal to or greater than this value, so it appears that very little correction is required for this system. This is probably due to the coaxial cable used for the PZT pins being approximately 30 feet longer that the optical fibers used in the VISAR system.

2. Strength Information

Because high quality data were obtained for 6061 aluminum, we can find the value for the HEL stress. The wave profile for our second Al shot is shown in Figure 22, and two-wave structure on the shock up side of the profile is clearly observed.

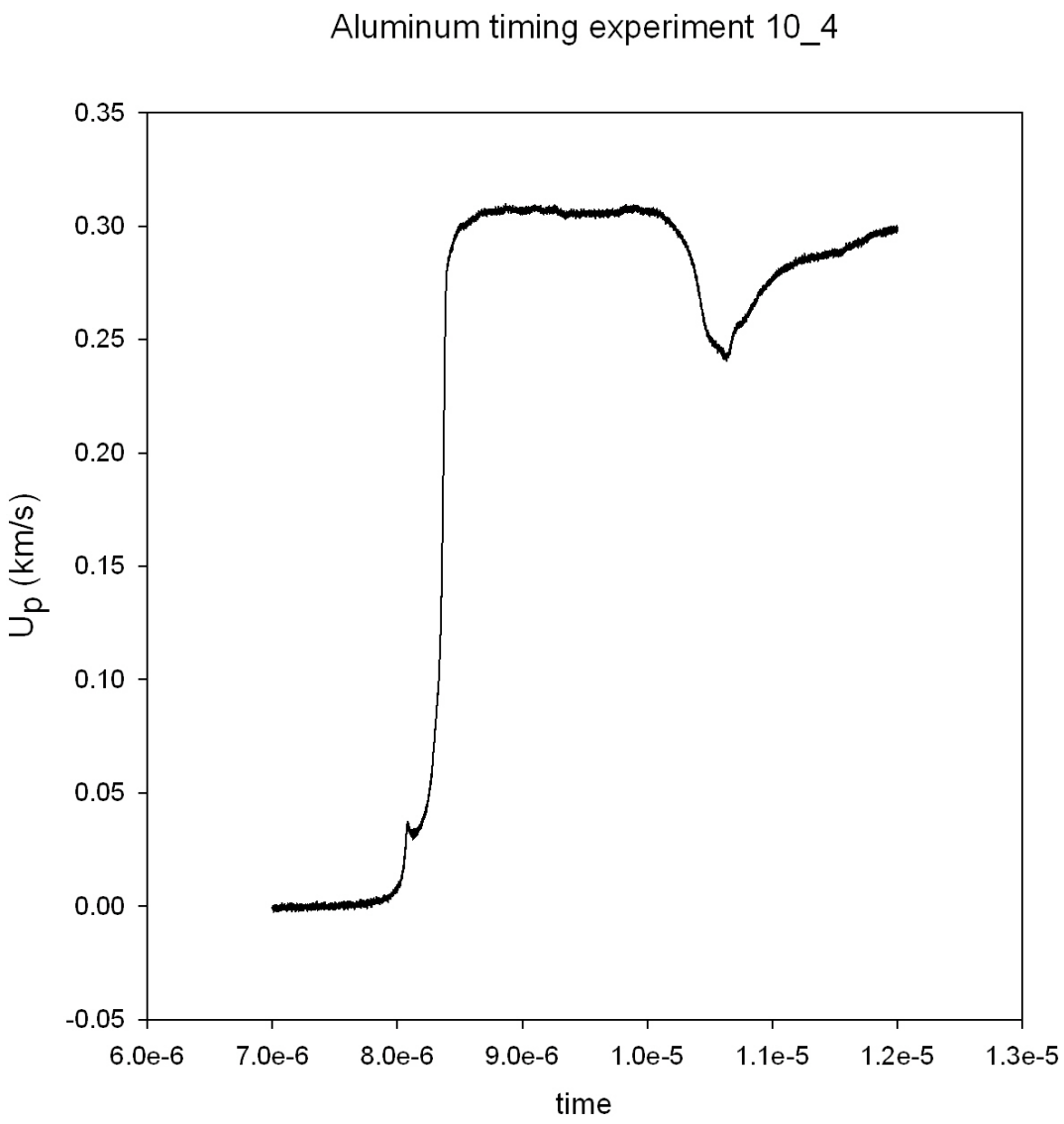

Figure 22. Wave profile from second AL6061 shot at NPS

The horizontal axis in this figure is time, and the vertical axis represents particle velocity. The wave profile shows a flat top indicating that a steady shock was obtained. A clear elastic precursor is obtained; some precursor decay is observed. Spall is observed late in the profile due to the free surface interaction. These signatures will be discussed in more detail. A small gas cushion effect is seen in the leading edge of the elastic wave, a result of some Helium gas blowing past the front projectile O-ring upon its exit from the barrel nanoseconds before impact.

We calculate the HEL from this data using the technique described above. First, the particle velocity at the peak of the elastic wave is measured; in this case, it is approximately 0.036 km/s at the peak. We use the measured longitudinal wave speed as given above (6.479 km/s), and then apply the momentum jump condition:

$$P - P_0 = \rho_0 U_S u_P$$

Where u_{FS} is the particle velocity at the top of the first (elastic) wave. This yields a value of 0.315 GPa. This is a typical value for aluminum.

B. CERAMIC HUGONIOT SHOTS

Next, we will describe the experiments done on the ceramic material using the results from the aluminum shots above to interpret the results. Experiments were done both at the NPS and at LANL. A higher performance single stage gun at LANL was used for two experiments to be able to reach higher pressure.

1. LANL Experiments

Los Alamos National Lab, in collaboration with NPS, performed two experiments on Corbit 98 samples from the NPS stock.

a. LANL #1

The first ceramic experiment performed at LANL was designed as a window shot at relatively high impact speed. A thin layer of aluminum was vapor plated onto a sapphire window, which was glued to the back side of the ceramic sample. The aluminized layer was used to reflect the laser beam for the VISAR diagnostic. Planned flyer velocity was 0.80 km/s, with 0.796 ± 0.003 km/s measured with an indicated tilt of 0.69 mrad. Diagnostics on this experiment included PZT pins, VISAR, and photonic Doppler Velocimetry (PDV). This suite of diagnostics provide very complete information on the shock conditions achieved in this experiment, and are somewhat more advanced than the current NPS diagnostic suite. The target was ground to a thickness of 3.055 ± 0.002 mm and lapped flat and parallel to a few microns. A Z-cut sapphire

impactor was used, which was measured to be 3.051 ± 0.0005 mm thick. The impactor was foam backed with a piece of 4.96 mm thick closed cell foam to provide a low shock impedance boundary at the back of the flyer.

The VISAR data from this experiment is of extremely high quality and clearly shows an elastic precursor. The plastic wave is somewhat ramped. This is probably due to fundamental properties of the ceramic that are beyond the scope of this research. However, from this transition point, the HEL was calculated. The method of calculation is described in a subsequent section. Timing information was used to calculate shock velocity. An initial density of 3.8635 g/cc was measured for this sample. Analyses for tilt corrections by LANL are added in the appendices. Transit time from flush pins was 0.2986 μs. From this data, the shock speed was calculated to be 10.34 km/s. From this measured shock velocity and the measured flyer velocity, with a known flyer Hugoniot, a particle velocity in the target was calculated using the above impedance matching method to be 0.426 km/s. VISAR data for this experiment is shown and discussed further in section IV.

b. LANL #2

A second shot performed at LANL focused on measuring spall strength. Because it was a spall experiment, no window was used. A 12 micron thick stainless steel foil was glued to the back side of the ceramic sample to allow observation of the free surface motion with VISAR and PDV. LANL reports an impact speed of 0.480 ± 0.003 km/s. A thicker ceramic sample was used than in the first LANL experiment with a measured thickness of 5.987mm. This will allow a more accurate measurement of shock velocity because it leads to a longer shock transit time in the sample. From this data, the shock speed was calculated to be 10.806 ± 0.203 km/s. As described above, particle velocity was found to be 0.243 km/s. Details of the spall strength calculation will be given below.

2. NPS Experiments

NPS ceramic experiments were done at relatively low stress conditions for two reasons. First, the performance of the NPS gun limits the maximum projectile velocity possible, and secondly the LANL experiments provide data at higher stress. Because these were the first experiments done at NPS to actually collect usable data, we were learning as we worked and developing new ways to build targets, align the gun, and carryout the projectile and impactor construction. In addition, the NPS experiments will be invaluable in constraining the elastic part of the shock compression response of this ceramic. Since this material has a very high elastic limit, this regime is very relevant for much of the penetration process.

a. Shot 10_3

The first ceramic experiment performed at NPS was designed to measure the spall strength of Corbit 98. A thin layer of gold foil was attached to the back side of the ceramic sample to reflect the VISAR laser. Planned flyer velocity was 0.24 km/s, and 0.242 km/s was measured with an indicated tilt of 2.58 mrad. The true tilt is really lower than the measured; the capability to accurately measure the stepped circular array of velocity pin heights requires better measuring instrumentation than is currently available at NPS. This causes a relatively large uncertainty in the calculated tilt—estimated to be greater than 0.8 mrad. Target thickness was 6.231mm in the center. Each surface of the target sample was flat, but with some tilt between surfaces approximately 30 μm. A ceramic impactor was used and was 3.176mm thick in the center. It also had about 30 μm of tilt between its faces. The impactor was foam backed with a piece of 4.96 mm thick closed cell foam. This foam backing was necessary to provide a very low shock impedance boundary at the back of the flyer so that a deep release wave is reflected.

VISAR data shows that the foil lost reflectivity shortly after shock breakout. This is probably due to imperfections in the ceramic surface causing ‘jetting’ that destroyed the reflectivity of the foil. Because of this, the spall signature was not recorded. But, we do get timing information that is used to calculate shock velocity.

We made a detailed comparison of the electrical signal delays and the optical signal delays from this data, using the measured longitudinal sound speed—10.55 km/s. Shear velocity was measured to be 6.18 km/s. Both of these values are typical for alumina ceramics of this density. To get the time correction between flush pins and the VISAR, we took there to be no timing correction needed. The difference in time between the tilt-corrected impact time from the flush pins and the first wave arrival at the back of the ceramic was 0.583 ± 0.05 μs. This leads to a measured shock speed of 10.68 ± 0.5 km/s. The impact time as determined from flush pins was 8.762 μs. The flush pins times were corrected for the fact that FP1 was 0.014 mm inset from impact surface, and FP2 was 0.013 mm inset. The measured projectile velocity was used for these corrections.

b. Shot 10_5

The second shot done on Corbit 98 at NPS was also the first done with a sapphire window. The window is used to keep spall from happening and provide an almost in-situ measurement of the particle velocity history. The 3" gun once again was used to throw an aluminum projectile a target plate containing the sample. A 3.126 mm thick piece of aluminum backed with foam served as the impactor. Velocity pins failed to record data, so projectile velocity is estimated from the gun performance curve. From the measured projectile mass of 357.2 grams and the breech pressure used—287 psi—the performance curve projects the impact speed to be 0.199 ± 0.01. Two flush PZT pins were used to record impact time. Sample thickness was 6.176 mm.

For this shot, high quality VISAR data are obtained, as shown in Figure 23. We observe a single shock wave, followed by a flat top. This indicated that we had a steady shock. This is followed by a release that originates at the back surface of the flyer, and then by two-dimensional release originating from the sides of the sample. This will be discussed in more detail.

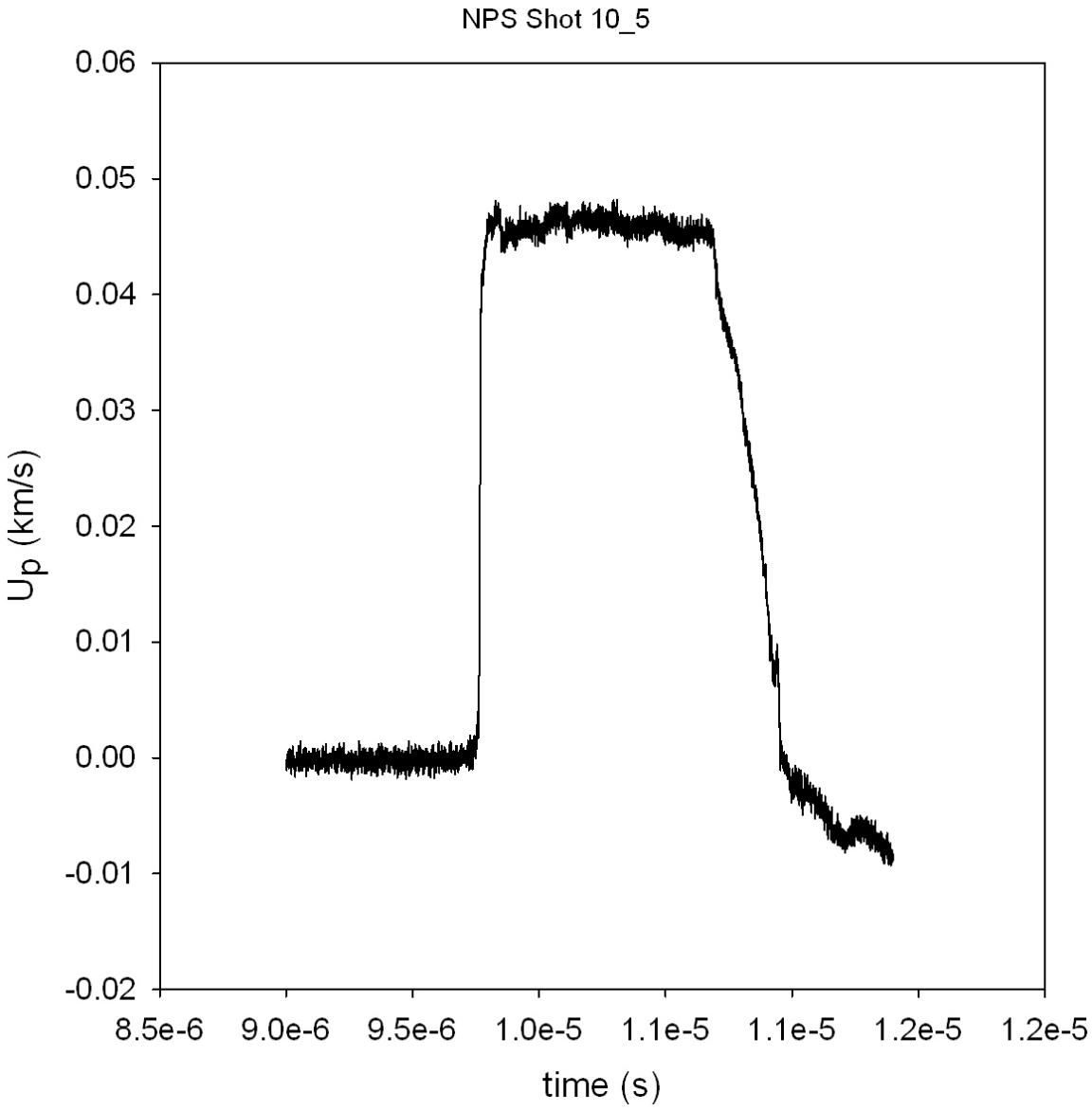

Figure 23. Wave profile for the second Ceramic shot at NPS

As in previous wave profiles, the horizontal axis displays time, and the vertical axis records particle velocity. The impactor was stood out about seven mm in front of the projectile nose, and so we see no evidence for a gas shock. Good flush pin data were obtained and corrected for offset to the impact surface. When this timing information was combined with the shock rise from the VISAR, a very high shock speed was calculated, much higher than is physically possible. Therefore, it is inferred that the ceramic sample was not coplanar with the impact plane defined by the target plate and

the flush pins. It's possible the sample moved after it was measured but before the glue was completely hardened. This experiment was very successful in that we obtained our first time-resolved shock information on this particular ceramic.

c. Shot 10_6

A third ceramic shot was performed at NPS, the primary purpose was to verify the results of the previous shot and obtain a value for shock velocity. The experimental setup was close to the previous shot. Velocity pins were used on this experiment, but data again was not obtained. We rely on the gun performance curve and the VISAR data to constrain projectile velocity. Flush pins show that projectile tilt was less than 1 mrad. A shock velocity of 10.59 ± 0.3 km/s was obtained. Very high quality VISAR data were obtained as shown in Figure 24.

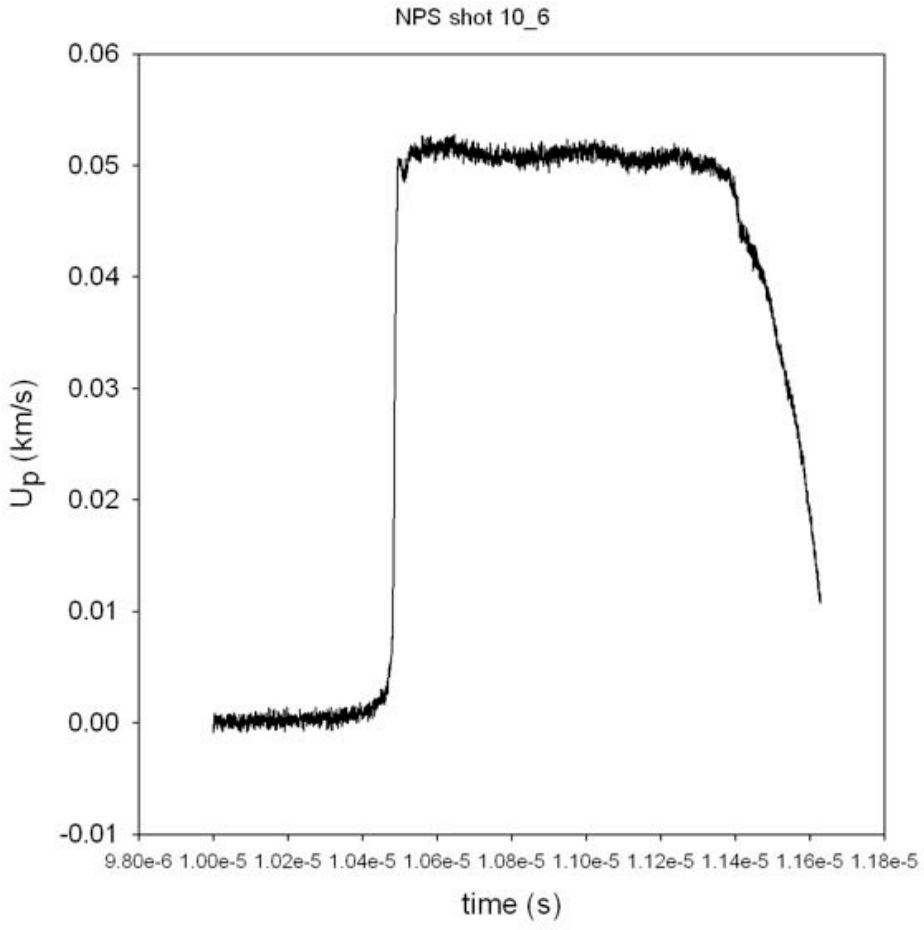

Figure 24. Data from experiment 10_6

From this data set, we can see clear evidence for a very flat impact, as evidenced by the very fast shock rise time. On the release side of the wave profile, we see evidence of the elastic/plastic response of the aluminum flyer, observed as a notch. Particle velocity was found to be 0.0508 km/s.

d. Shot 10_7

This was the final experiment done in support of this research on the NPS gas gun. This was designed to be a window experiment at higher stress than those described above, and to fit in between the highest NPS experiment and the lowest LANL experiment. To obtain higher stress, we used a single crystal (z-cut) sapphire impactor, and a higher impact velocity. Measured impact velocity was 0.306 km/s, shock velocity was 10.59 km/s, and calculated particle velocity was 0.161 km/s. The data from this experiment is shown in Figure 25 and is of very high quality.

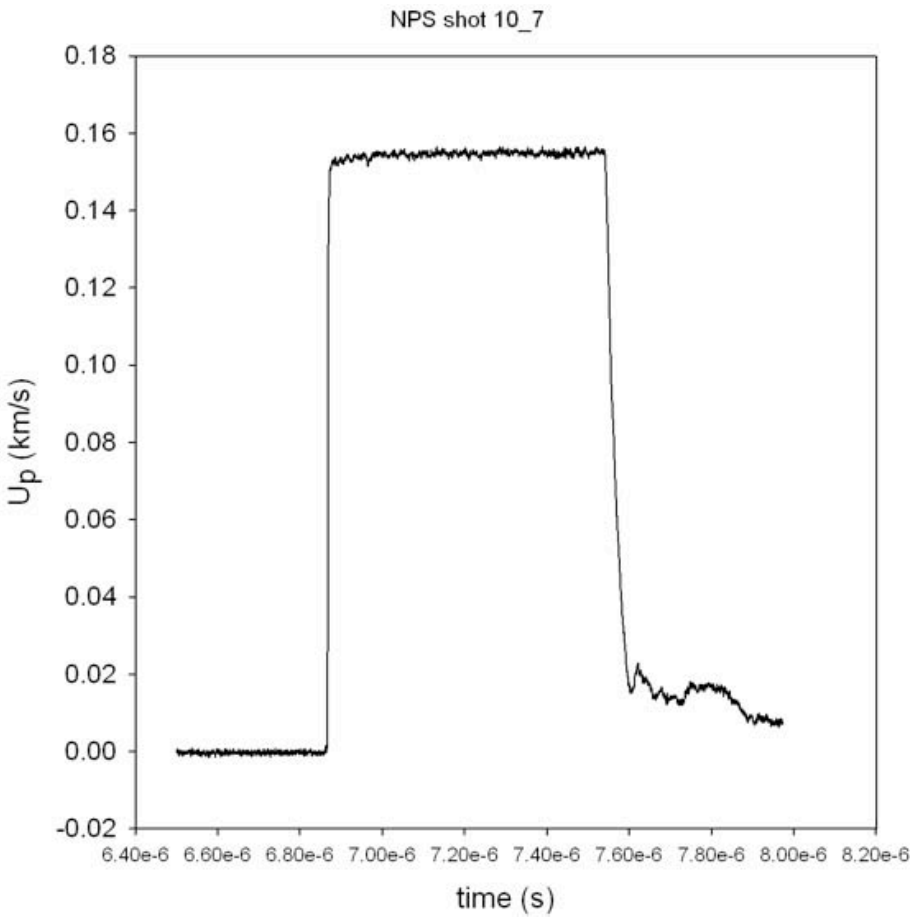

Figure 25. Data from experiment 10_7 is of very high quality

Note that this data shows a significantly higher interface velocity indicating that a higher stress state was achieved. We note also that this interface state is very close to constant velocity indicating we had a one-dimensional steady state until the release from the back of the flyer reached the target/window interface. Calculations show we obtained a stress state of 6.57 GPa. From this wave profile, we also see a significantly faster shock rise time than is our lower stress experiments. In fact, the rise time is fast enough that we needed to add a 'lost fringe' when analyzing the interferometer data. This happens when an interference fringe moves faster than the VISAR system can resolve in time. This is also indicative of having a very flat impact and a higher stress state. We also note that the release wave that drops stress falls very quickly. This appears to be a characteristic of alumina based ceramics and single crystal sapphire.

IV. DISCUSSION OF RESULTS

A. HUGONIOT RESULTS

Because polycrystalline ceramic materials are made using a sintering process, some variability in their properties is to be expected. This means that we must be careful in our comparisons with previous data on similar ceramics. As shown above, initial density is a key property that appears to be useful in making such comparisons

As mentioned above, ceramics can have different starting properties, and this can affect their shock properties. We show in Figure 26 for plastic shock data on ceramics, all with a reported initial density between 3.8 and 3.9 g/cc. This shows that even for ceramics with relatively similar initial density we can see significant scatter in the shock data. For this reason, we select literature values to compare with carefully. We compare to Coors AD995 data, as this has the closest initial density to the Corbit material, and has very similar initial sound speeds.

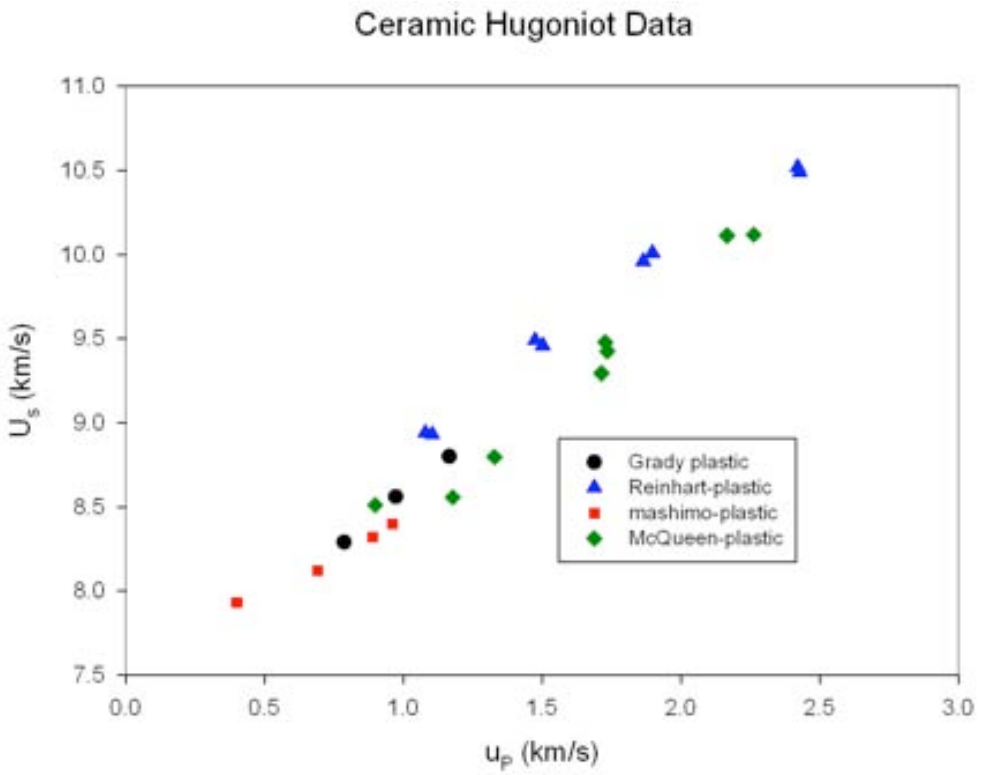

Figure 26. Ceramic data from the literature shows relatively large scatter (After [11, 12, 14, 15]).Results for ceramics with very different initial densities show even more scatter than shown in Figure 26.

1. Hugoniot Data for Similar Materials

Dennis Grady [11] characterized AD-995, which is a ceramic produced by Coors Porcelain Company. This material is quite similar to Corbit 98. Other properties, such as sound velocity, are also very similar, as shown in Table 1 on page 17. Grady also measured a value for the HEL of this material; and this will be discussed.

Gust and Royce [10] examined various ceramics and found different longitudinal sound speeds for different initial density. Among the materials they studied, the closest match to our ceramic in initial density is 'hot pressed' Al_2O_3 ceramic material made by the Carborundum company. Initial properties for this material are shown in Table 1 and are a close match to our material.

In addition, more data on the Coors AD-995 ceramic has been generated recently by Reinhart and Chhabildas [12]. We will include their data in our Hugoniot

comparisons. Marsh et al. [15] and Ahrens et al. [17] reported Hugoniot results for ceramic materials with similar initial density. We will also compare to some of this data.

Our measured values for elastic Hugoniot data are summarized for all of our experiments in Table 4:

Table 4. NPS and LANL Hugoniot for Corbit-98 ceramic

Shot	Impact Velocity (km/s)	U_S (km/s)	U_p (km/s)	Stress (GPa)	Type
NPS 10_3	0.242	10.68	0.121	4.96	FS
NPS 10_5	0.199	10.60	0.054	2.21	SW
NPS 10_6	0.191	10.59	0.051	2.09	SW
NPS 10_7	0.306	10.59	0.161	6.57	SW
LANL 1	0.796	10.34	0.426	17.03	SW
LANL 2	0.48	10.806	0.243	10.15	FS

Note that shots typed as FS are free surface, and those typed as SW are performed with a sapphire window.

In Figure 27, we plot shock velocity against particle velocity for the data discussed in Table 4, along with our longitudinal sound speed datum, as well as plastic shock from sources discussed. As can be seen, there is still considerable scatter in results as compared to similar data for elements. But overall, we see reasonable agreement. The elastic branch of the Hugoniot in particular is difficult to measure. This is because the slow projectile velocity causes small distance uncertainties to lead to large time uncertainties. And, the very high ceramic shock velocities cause very short shock transit times in the sample, which can be hard to measure accurately.

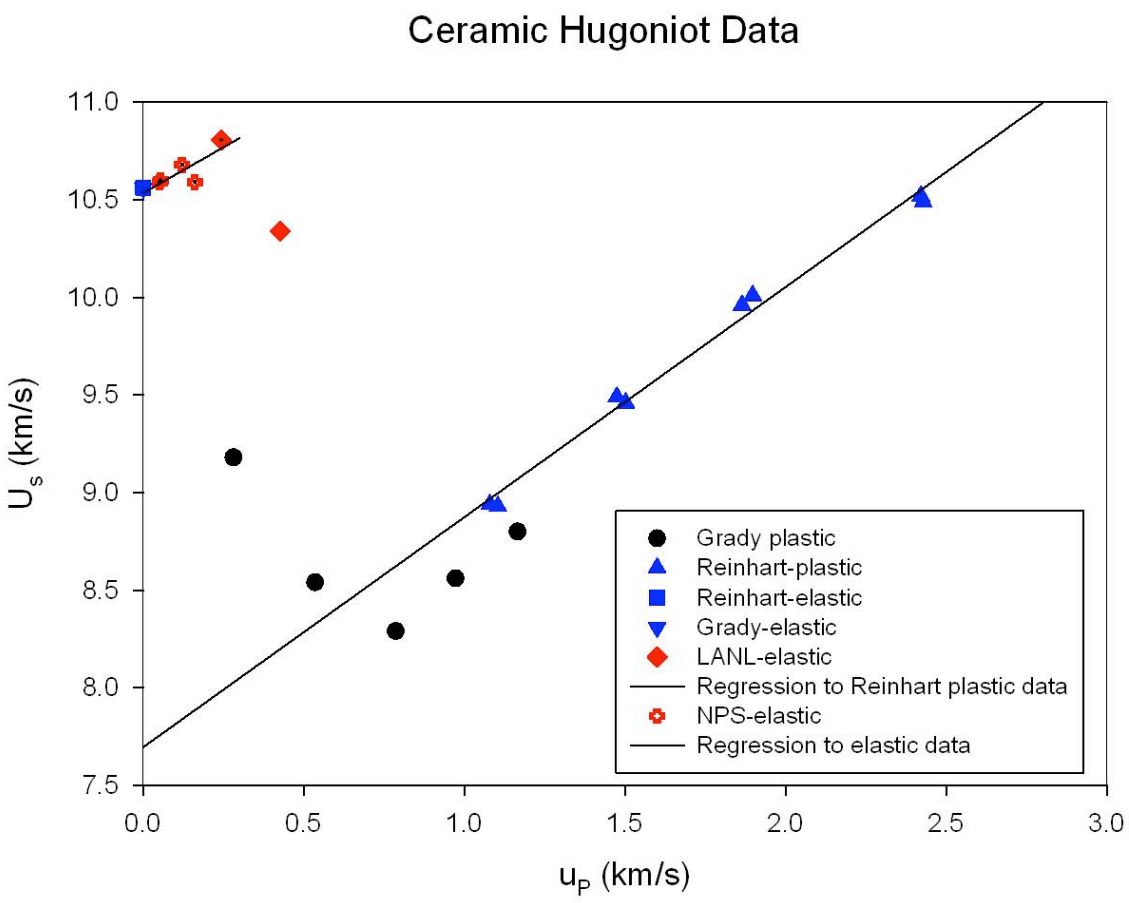

Figure 27. Hugoniot Plot of NPS and LANL data

We can also show this data in pressure-volume space. In Figure 28, we show our results plotted along with selected results from the literature for similar ceramics (see previous discussion). We see reasonable agreement, with relatively large uncertainties for reasons discussed.

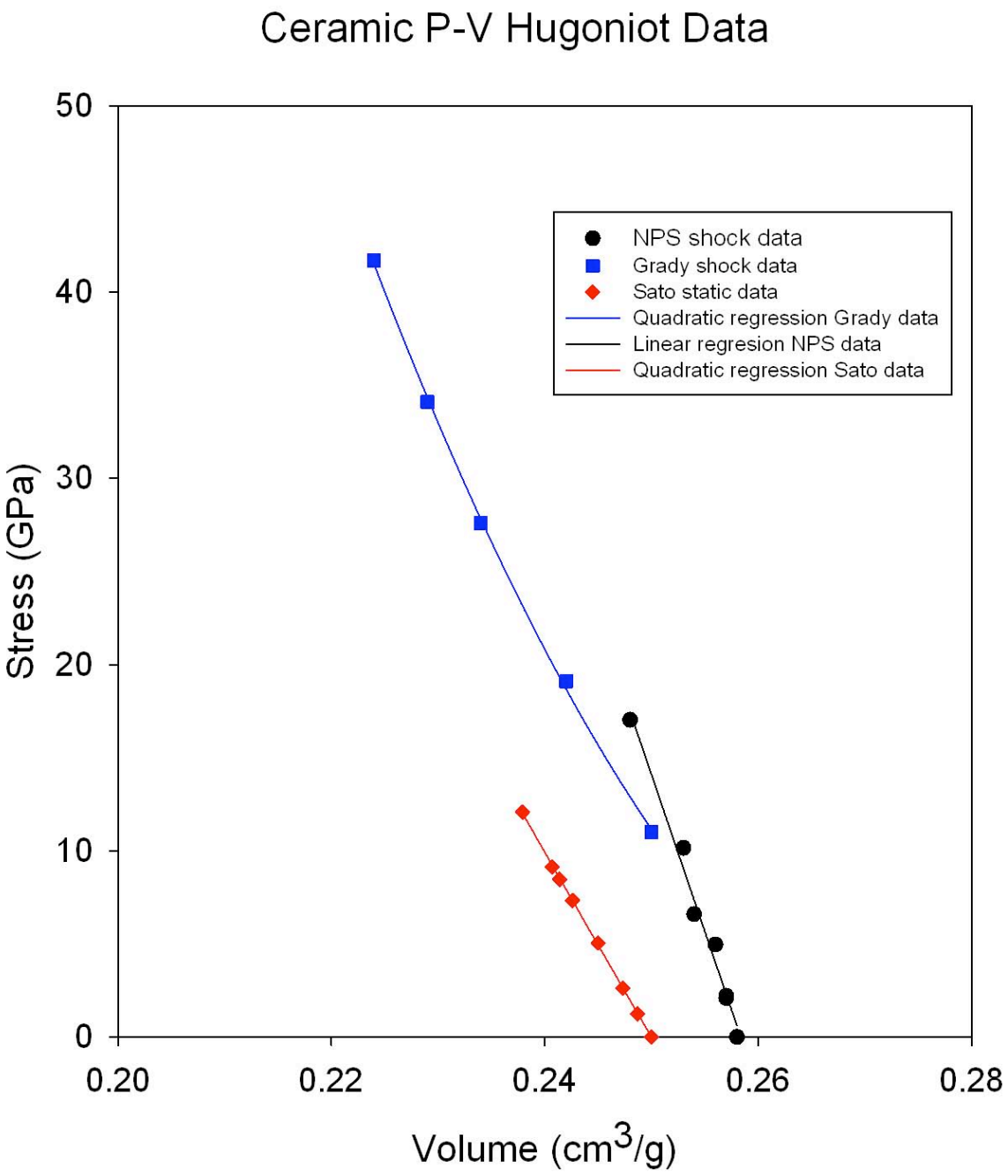

Figure 28. Hugoniot plot in P-V Space (After [12, 18])

Here, we also show static data from Sato et al. [18] collected using a cubic anvil high-pressure apparatus, and as plotted by Grady [12]. This data is in a state of hydrostatic compression; the shock data is in a more complex stress state. As stress increases, we see our data systematically differing from that of Grady. This is because

the Grady data—except for the lowest point—is in a state of plastic deformation, but our data is all in elastic deformation. The point where the quadratic fit to the Grady data and the linear fit to our data intersect is the yield point. This is discussed in further detail, but we clearly see that this intersection will be at approximately 7-9 GPa.

2. Uncertainty Analysis for Hugoniot Data

We have looked at several potential sources of uncertainty in our quantitative Hugoniot results. Here we'll briefly discuss the principal sources of uncertainty, which are in measured *distances* and *times.*

We are able to measure distance with an electronic length-measuring device to 1-2 mm. But this is not the limiting factor. The real limit for our ceramic samples is in the surface flatness, and how parallel the front and back surfaces are to each other. For the sample used in these experiments we estimate this uncertainty to be 12 mm out of a total thickness of 6.134 mm. We also estimate the time uncertainty to be 15 ns in shock transit time, which for experiment 10_7 was 0.579 μs. Using these values we estimate we are measuring thickness to about 0.2 % and transit time to about 2.5%. The reasons we have a relatively large uncertainty in transit time have been mentioned—because of very slow projectile velocity, very fast shock velocity in the sample, and relatively short transit time. We can use these fundamental values to see how errors propagate into our measured value for shock velocity. The equation below, which assumes a Gaussian distribution of uncertainty, allows us to calculate fractional uncertainty in shock velocity:

$$\frac{\Delta U_S}{U_S} = \sqrt{\left(\frac{\Delta x}{x}\right)^2 + \left(\frac{\Delta t}{t}\right)^2}$$

This result shows us that the estimated uncertainty in U_s is about 2.51%, or just slightly more than our assigned uncertainty in transit time. We can also estimate uncertainty in our calculated values for shock stress. We use the result above for fractional uncertainly in shock velocity along with that for flyer velocity. We estimate we can measure flyer velocity for shot 10_7 to be 0.003 km/s with a U_D of 0.308 km/s. If

we assume a very small contribution from the measured initial density (a very good assumption), then we can calculate uncertainty in stress from:

$$\frac{\Delta P}{P} = \sqrt{\left(\frac{\Delta U_S}{U_S}\right)^2 + \left(\frac{\Delta U_D}{U_D}\right)^2}$$

The result is the uncertainty in stress is about 2.69% for this particular experiment. It is somewhat worse for other NPS experiments because of a larger uncertainty in projectile velocity.

3. Strength Results

One principal goal of this research was to determine the compressive dynamic yield strength for Corbit ceramic. In order to do, this we must shock to a pressure state above that yield point. Because this is difficult to do on the NPS gas gun, we use the results from the LANL experiments to directly measure the yield point. As previously described, this is the point at which the elastic and plastic Hugoniots in P-V space cross. Both LANL experiments show evidence for two wave structure. Because of the (presumably) complex nature of the yielding process in polycrystalline ceramics, the wave structure at stresses slightly above the HEL (yield point) is also complex. However, in both LANL experiments, we see a clear elastic precursor wave. Because one experiment had a sapphire window and the other had a free surface, we use different analysis techniques to find the stress state associated with this particle velocity. We start with the first LANL experiments, which had a window. Shown in Figure 29 is the wave profile as measured for this shot.

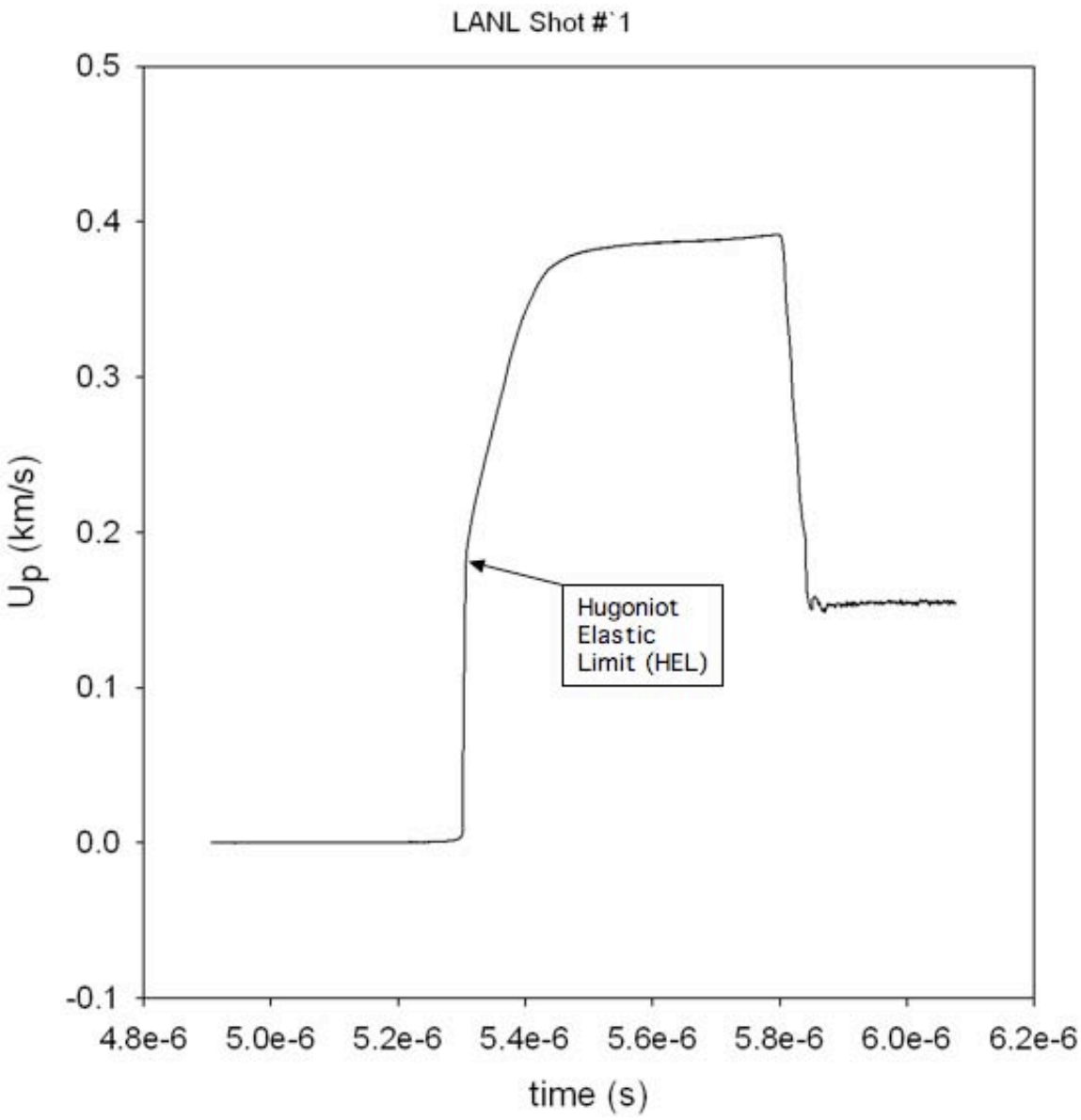

Figure 29. Wave profile from LANL shot 1

We see a clear transition from elastic response to plastic response at a particle velocity of about 0.186 km/s. Above this particle velocity, we see a very ramped plastic wave indicating that the yielding process is progressing, but in a complex manner. To find the pressure state at this particle velocity, we must take into account the fact that there is a sapphire window at the measurement interface, and the state there is a reshock. That is, the presence of the window causes a wave to be reflected back into the ceramic

sample, taking the sample to a higher pressure than that behind the shock that initially moved through the sample. This process is illustrated in Figure 30:

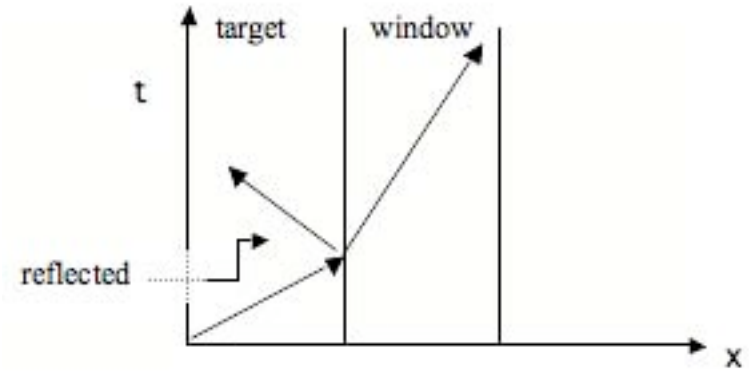

Figure 30. Wave interactions at the target/window interface

This *reshock* occurs because the window has slightly higher shock impedance than the window. To correct for this, we first use a technique that is easily derived:

$$P_b = \left(\frac{2Z_b}{Z_a + Z_b} \right) P_a$$

Where P_a is the shock state behind the initial shock in the ceramic target and P_b is the reshock state caused by the window interaction. Za and Zb are the shock impedances of the sample and window at these conditions. Shock impedance is defined as $Z = \rho_0 U_s$. We have enough information to find this pressure. The target shock impedance is found to be 39.95 and window impedance is found to be 45.38. Using the momentum jump condition, P_b is determined to be 8.44 GPa. Substituting into the above equation, we find **P_a= 7.96 GPa**. This is HEL for Corbit ceramic as determined from this experiment.

This calculation can also be performed with another analysis of the P-up diagram. Figure 31 provides the case for a lower impedance target (ceramic) with an interface with a higher impedance window (sapphire). Notice that ceramic is considered a high impedance material, but sapphire is higher still.

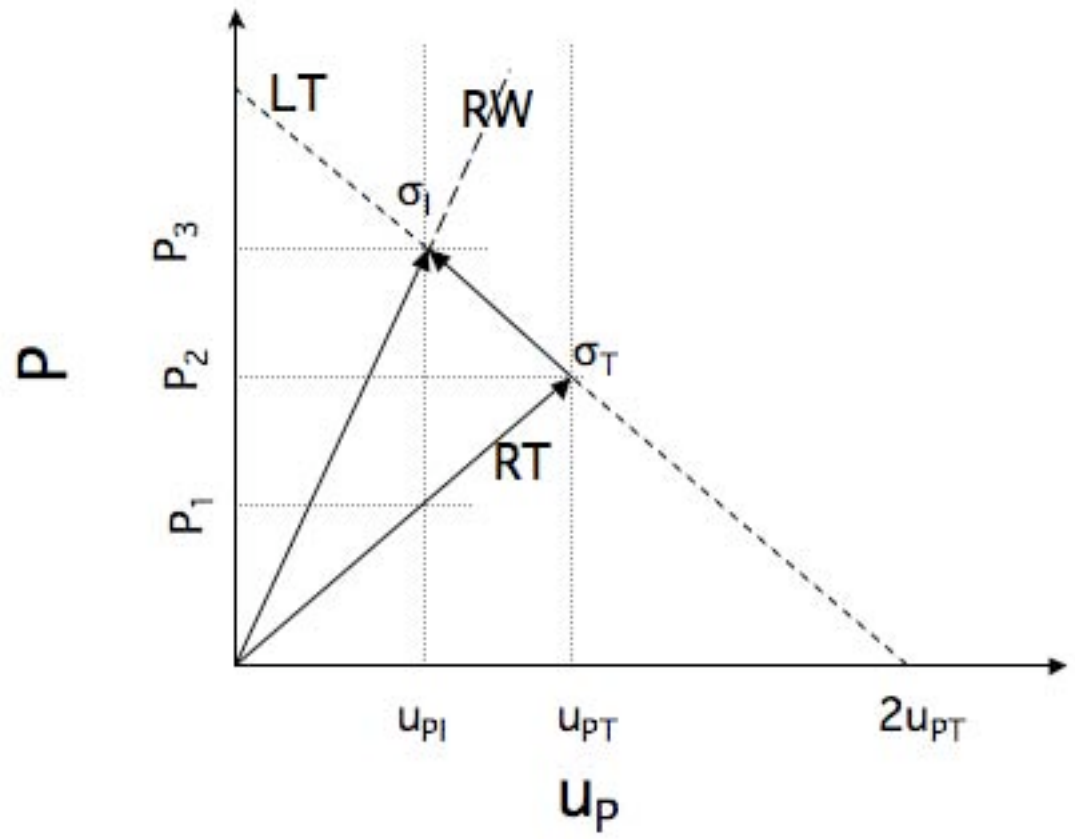

Figure 31. Cartoon P-up Diagram for Ceramic-Sapphire Interface

In this figure, curves labeled “RT” and “LT” symbolize ceramic Hugoniots for right-going and left going waves in the target, respectively, while the curve labeled “RW” is symbolic of a right-going wave in the sapphire window. Curves with positive slope represent a right-going wave, and negative slope implies a left-going wave. The most crucial point in this analysis is understanding that the VISAR measures data at the point (u_{PI}, P_3). The particle speeds of interest are the particle speed at the interface, the particle speed in the target, and twice the particle speed in the target denoted u_{PI}, u_{PT}, and $2u_{PT}$ respectively. Notice that $u_{PI}<u_{PT}<2u_{PT}$. The pressure, or stress states, of note are designated as P_1, P_2, and P_3. We use the known sapphire Hugoniot equation of state from Marsh [15],

$$U_S = 11.19 + 1.0 * u_P$$

To find the value of P_3, or the stress state at the interface:

$$P_3 = \sigma_I = \rho_{0S} * U_{SS} * u_{PI};$$
$$P_3 = \rho_{0S} * (11.19 + 1.0 * u_{PI}) * u_{PI}$$

Where ρ_{0S} is the density of sapphire (3.985 g/cc) and u_{PI} can be read off the wave profile VISAR record for this shot. Assuming a particle speed of 0.187 km/s at the transition point as measured, the interface stress state is found to be 8.48 GPa. Knowing the numerical value of P_3, we can solve for the particle speed in the target, u_{PT}:

$$P_3 = 2 * u_{PT} * U_{SC} * \rho_{0C} - U_{SC} * u_{PI} * \rho_{0C};$$
$$u_{PT} = \frac{P_3 + U_{SC} * u_{PI} * \rho_{0C}}{2 * U_{SC} * \rho_{0C}};$$

Where ρ_{0C} is the density of ceramic (3.8635 g/cc measured by LANL for this shot), U_{SC} is the shock speed in ceramic (which we assume is the longitudinal sound speed 10.55 km/s). Inserting values and solving, u_{PT} comes out at 0.198 km/s. Finally, to find P_2 and P_1, or the stress state at the HEL, we use the momentum jump condition:

$$P_2 = \rho_{0C} * U_{SC} * u_{PT};$$
$$P_1 = \rho_{0C} * U_{SC} * u_{PI};$$

Inputting the values listed above on the right side of the equation, the HEL is found to be 8.1 GPa. Notice that this value is consistent with the originally defined relationships: $0.187 = u_{PI} < 0.198 = u_{PT} < 0.396 = 2u_{PI}$ and $7.6 = P_1 < 8.1 = P_2 < 8.48 = P_3$. This mode of analysis provides a more complete understanding of the interface motion and the various stress states within the system. As waves continue to propagate in the materials, subsequent wave interactions occur, and each is just as complicated as the one examined above.

For the second LANL experiment, analysis is simpler. This is because we have a free surface boundary condition in this experiment. We must assume that the free surface approximation is correct. That is, we assume that the measured free surface velocity is twice the particle velocity in the target. This approximation is not rigorously true for high pressure, but is a reasonable approximation for our purposes. Data for this experiment is shown in Figure 32:

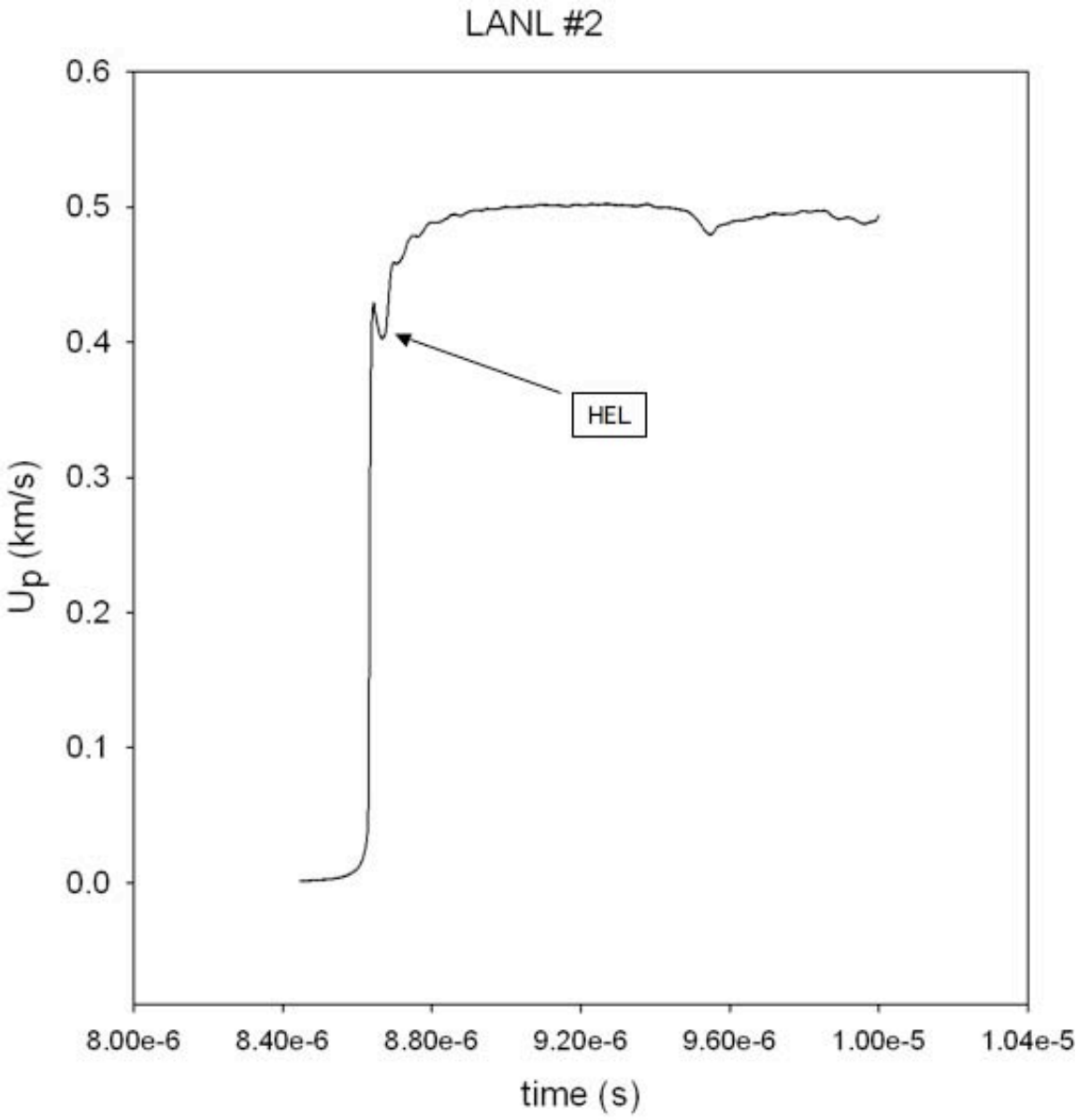

Figure 32. Wave profile from LANL shot 2

A clear elastic wave is observed for this experiment with a peak particle velocity of 0.428km/s. Note that this wave profile is somewhat different than that shown for the first LANL shot. This is because this shot had a free surface rather than a window. Wave interactions at the surface being observed by the VISAR are somewhat different leading to this difference in appearance. We now need only apply the momentum jump condition to find the pressure at the particle velocity.

$$P - P_0 = \rho_0 U_S u_P$$

Using the measured elastic shock velocity of 10.806 km/s, the particle velocity from above and the correct value for initial density leads to an HEL value of **8.27 GPa**.

Our two measured values for HEL are in close agreement

4. Spall Strength

Data from the second LANL shot can also be used to obtain the value for strength in tension. This is also called spall strength. As may be seen from the wave profile for this experiment, there is a dip in particle velocity late in time. This carries information about the spall strength. Figure 33 shows a distance time diagram for how tension is generated in a target sample using wave interactions.

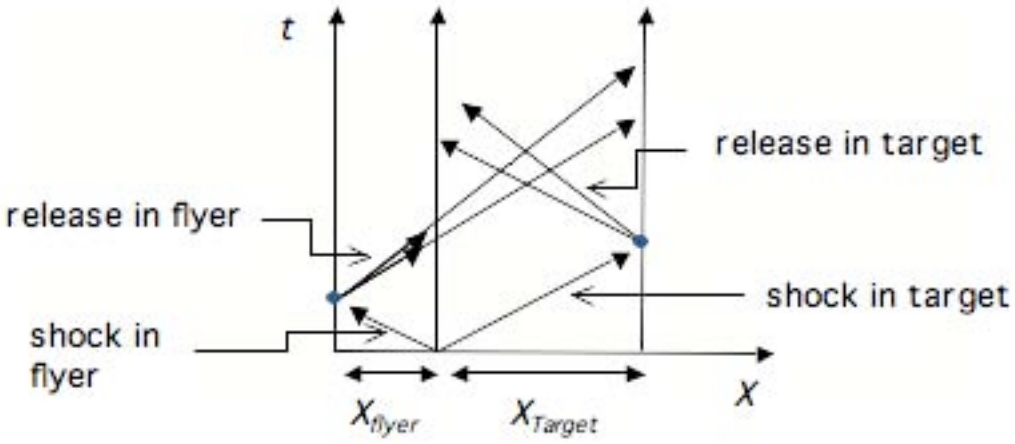

Figure 33. X-t diagram showing wave interactions that lead to dynamic tension

Information about spall is carried from the region of tension which is in the bulk of the sample to the surface observed by the VISAR by waves. The kind of wave profile expected for this kind of experiment is shown in Figure 34:

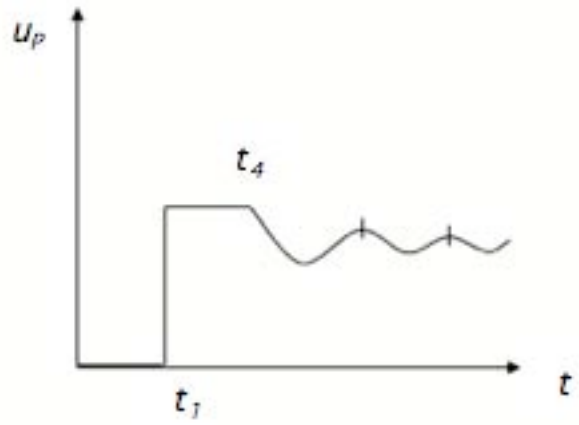

Figure 34. Generic wave profile for a spall experiment

The particle velocities after time t4 contain the information about spall. We clearly see these features in the second LANL experiment.

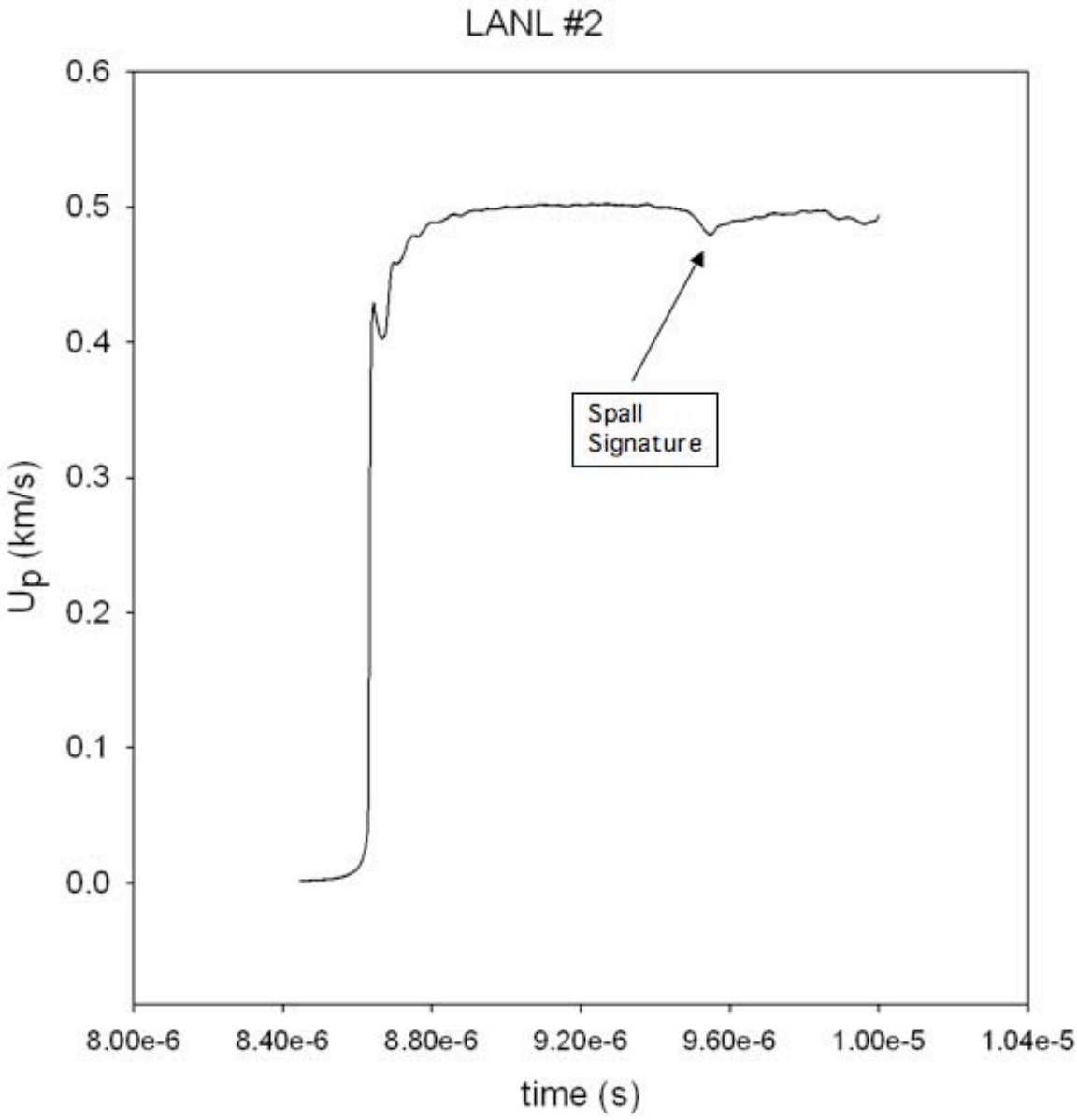

Figure 35. Wave profile for second LANL shot

In the second LANL experiment, a relatively thin flyer was used to impact a ceramic target. Here the flyer was Z-cut single crystal sapphire 4mm thick, and the target was Corbit ceramic approximately 6.15 mm thick. The reflected release wave from the target free surface and the reflected release wave from the back surface of the flyer interact approximately in the center of the target material. This causes a local state of tension to be created as described above. If this tension exceeds the spall strength of the

sample, it will fail and separate into two pieces. At the stress condition of this experiment, we expect that the spall strength of the ceramic will be easily exceeded. This is observed to be true by looking at the late time particle velocity record for this experiment. There is a clear 'dip' indicating that the sample has spalled. We can find an approximate value for the spall strength by use of the momentum jump condition as described.

The wave speed C requires some thought because the failure mechanism for a ceramic is almost certainly brittle failure and cracking. In this case, it is not rigorous to use bulk sound speed as would be done for a more ductile failure material. Because we are only looking for an approximate value for spall strength, we still proceed to use bulk sound speed, and this will cause a small error to exist in our calculated strength. In future work, we will revisit this issue. The value of Δu_{FS} is taken from the wave profile by subtracting the value of particle velocity at the bottom of the dip from the peak value. We find this difference to be 0.018 km/s. The bulk sound speed was calculated to be 7.80 km/s. Putting these values into the above equation yields a spall strength of 0.271 GPa. This is 2.71 kbar, and indicates that as expected it does not take much tension to cause this particular ceramic to spall. Grady [11] shows a value for a similar but higher density ceramic of about 5 kbar.

V. CONCLUSIONS

The work performed in this thesis provides fundamental dynamic material properties for the ceramic material known as Corbit 98. Results for dynamic yield point (HEL) and sound speeds are summarized in Table 5:

Table 5. Summary of results

Experiment	σ_{HEL} (GPa)	C_L (km/s)	C_S (km/s)
LANL 1	7.96 ± 1.5	n/a	n/a
LANL 2	8.27 ± 0.8	n/a	n/a
Sample 1	n/a	10.543	6.138
Sample 2	n/a	10.555	6.180

Each shot also contributes a single point to the Hugoniot Equation of state, as shown in Table 5. Using our data for elastic state, we find a best fit Hugoniot of:

$$U_s = 10.53 + 0.936 u_p$$

There is still a fair amount of uncertainty in this equation, and a few more shots to anchor its reliability are recommended. The summary graph for our Hugoniot information, as compared to some selected literature results, is shown in Figure 36.

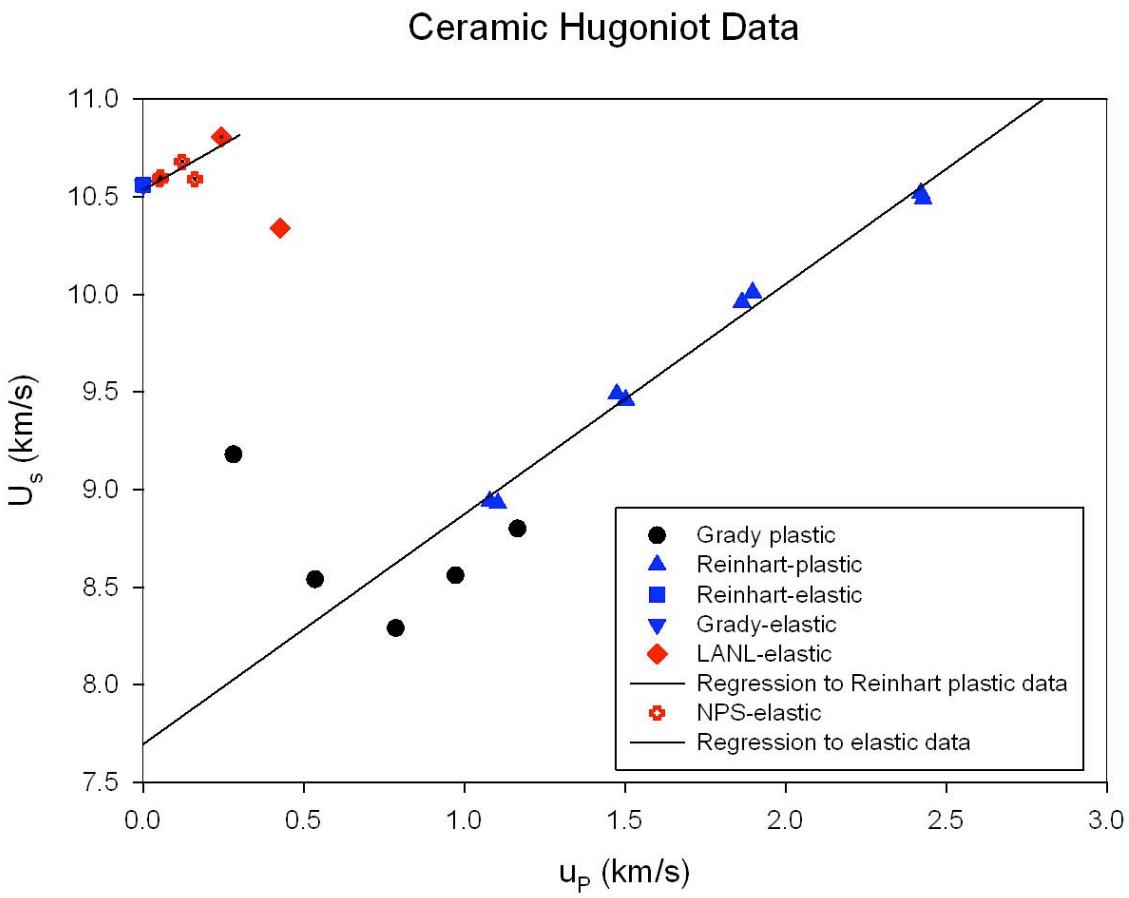

Figure 36. Compiled Hugoniot Data for Ceramic (After [12, 13])

These represent, to the best of our knowledge, the first Hugoniot data for this particular ceramic. Note that we have only measured the Hugoniot in elastic states of compression. The two LANL experiments actually contain information on plastic response as well, but the plastic waves are very dispersed in time. These will be analyzed as future work. To obtain fast rising plastic waves will require experiments at yet higher stress. A few of these are recommended for future research but are beyond the scope of this research. To reach to higher stress states will require the use of a higher performance gun. This data, once obtained, will allow a comparison to be made between the Corbit ceramic and the Coors AD995, as studied by Grady [11] and Reinhart [12]. For now, we use the plastic shock data of Reinhart [12] to define the plastic Hugoniot.

We have also successfully determined, for the first time, the spall strength of Corbit 98 ceramic, and found a value of 2.71 kbar. This clearly illustrates a principal technical issue with the use of alumina based ceramics as armor materials; they are very strong in compression, but very weak in tension. This seriously affects their multi-hit capability for armor applications. Specifically, at the Ceramic-Dyneema interface, a release wave is reflected from the interface back into the ceramic. This wave results from Dyneema's lower impedance. This effect is the reciprocal of the reshock that occurs in material at an interface with higher impedance. Interactions between such release waves will ultimately lead to tension in the ceramic, and spall separation if the spall strength is exceeded. The spall strength is a fundamental property of the material, which can vary with unloading rate, but for our purposes can be treated as being approximately constant. In computer simulations, it is easy to keep track of the stress state in each cell, and allow spall damage to occur if the tensile stress exceeds our measured value for the spall strength. Theoretically, if the second layer had higher impedance than the ceramic, then the ceramic would not enter a tension state until many wave interactions later. This could prevent failure from spall; however, a wave-spreading high impedance material does not exist.

The ideal first layer for our armor concept would be a material that was very strong in compression (had a high HEL) and still relatively strong in tension. This ideal material would also be ductile so that it would flow plastically to high values of strain, and not crack readily. Such materials do not currently exist, but research is ongoing to develop them. Bulk amorphous metals are now being produced in research quantities that have ductile dendritic inclusions that are able to limit the distance a crack can run in the brittle phase. This increases overall system ductility. Materials like this may be available in the near future and would be ideal for our application.

Using these new values for material properties, simulation models can now be improved for use in hydrodynamic computer codes. By adjusting the values used by Ong [1] at NPS, new computer simulations can now be done using the Johnson-Holmquist model with better input parameters [16]. Similarly, the input parameters for the spall model can also be refined based on this research. The equation of state (EOS) for the

ceramic layer of our composite armor system can also be refined based on these data. These simulation results can be compared to existing and new integral test results. These refinements will be left for future research.

APPENDIX-LARGE WAVE PROFILES

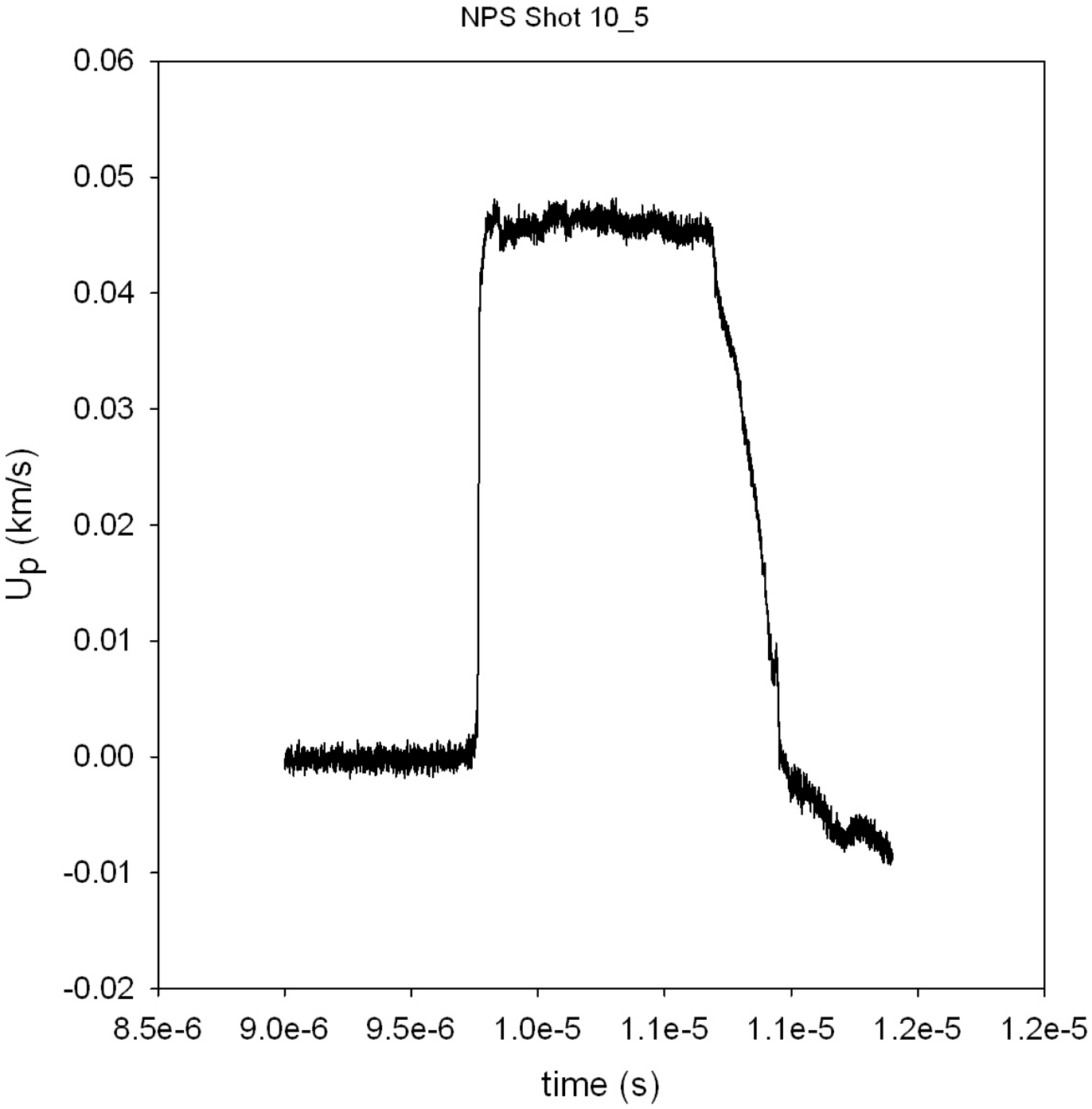

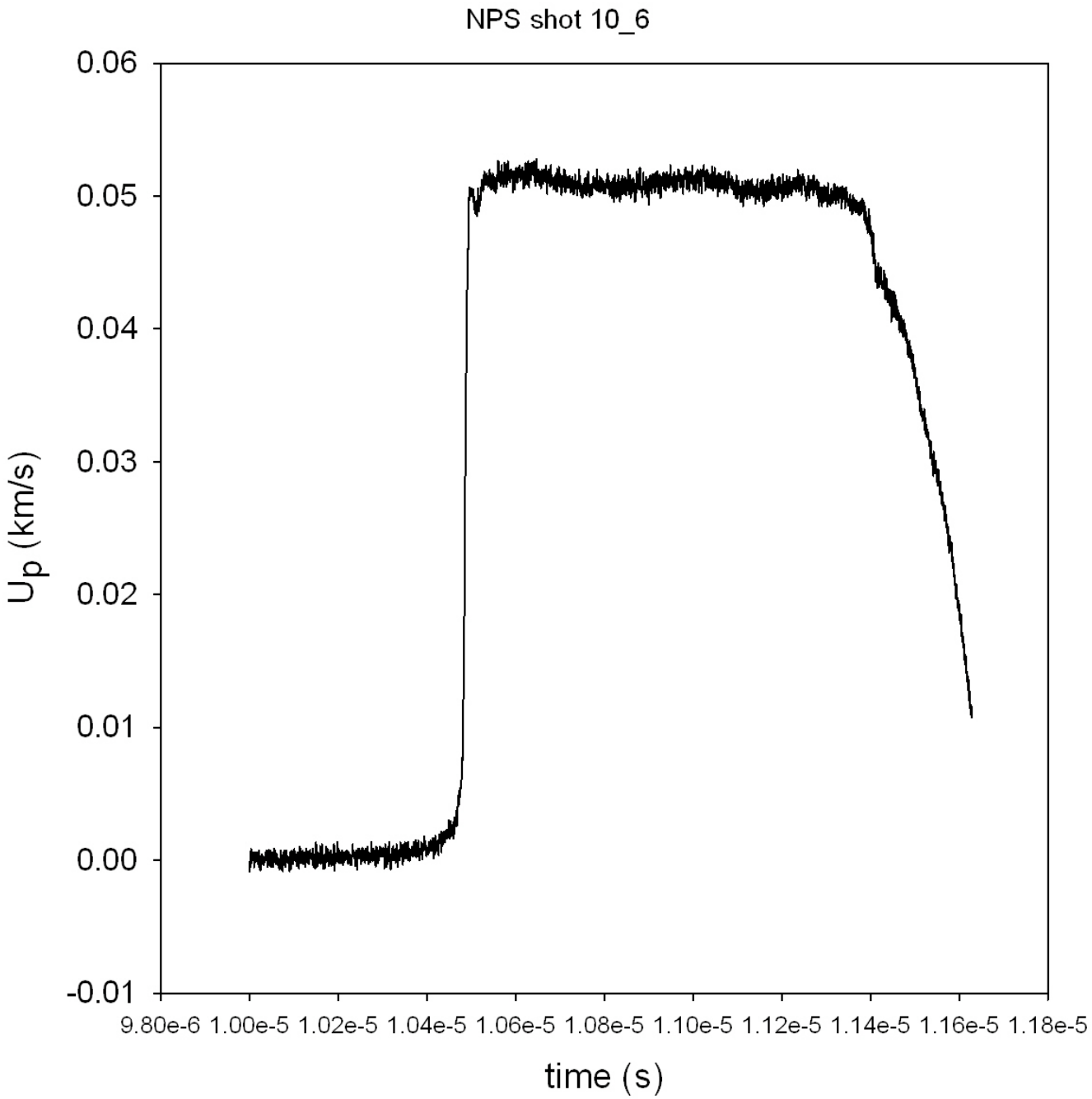
NPS shot 10_6
0.06
0.05
0.04
0.03
0.02
0.01
0.00
-0.01
U_p (km/s)
9.80e-6 1.00e-5 1.02e-5 1.04e-5 1.06e-5 1.08e-5 1.10e-5 1.12e-5 1.14e-5 1.16e-5 1.18e-5
time (s)

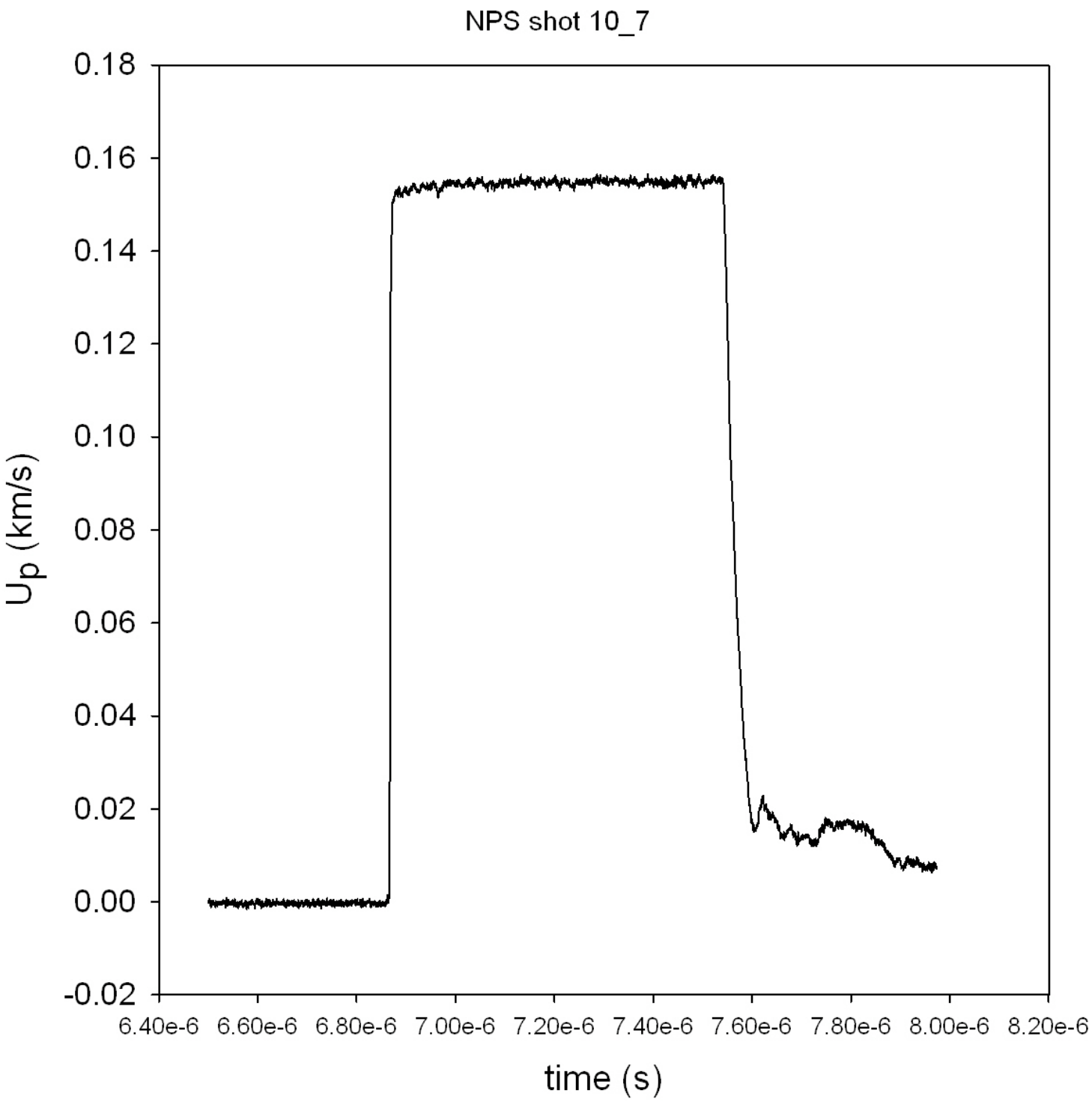
NPS shot 10_7
0.18
0.16
0.14
0.12
0.10
0.08
0.06
0.04
0.02
0.00
-0.02
Up (km/s)
6.40e-6
6.60e-6
6.80e-6
7.00e-6
7.20e-6
7.40e-6
7.60e-6
7.80e-6
8.00e-6
8.20e-6
time (s)

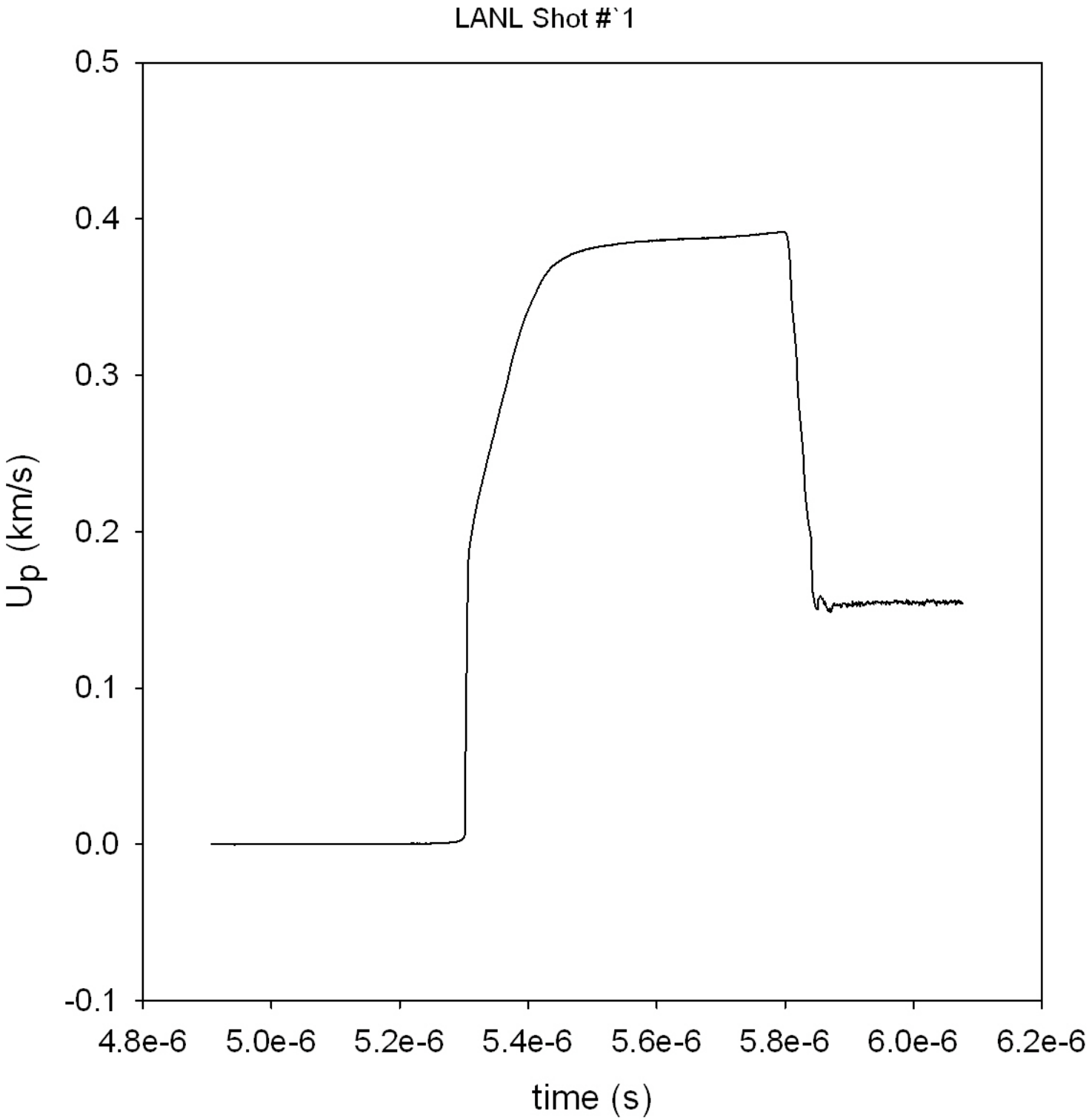
LANL Shot #`1
0.5
0.4
0.3
0.2
0.1
0.0
-0.1
Up (km/s)
4.8e-6
5.0e-6
5.2e-6
5.4e-6
5.6e-6
5.8e-6
6.0e-6
6.2e-6
time (s)

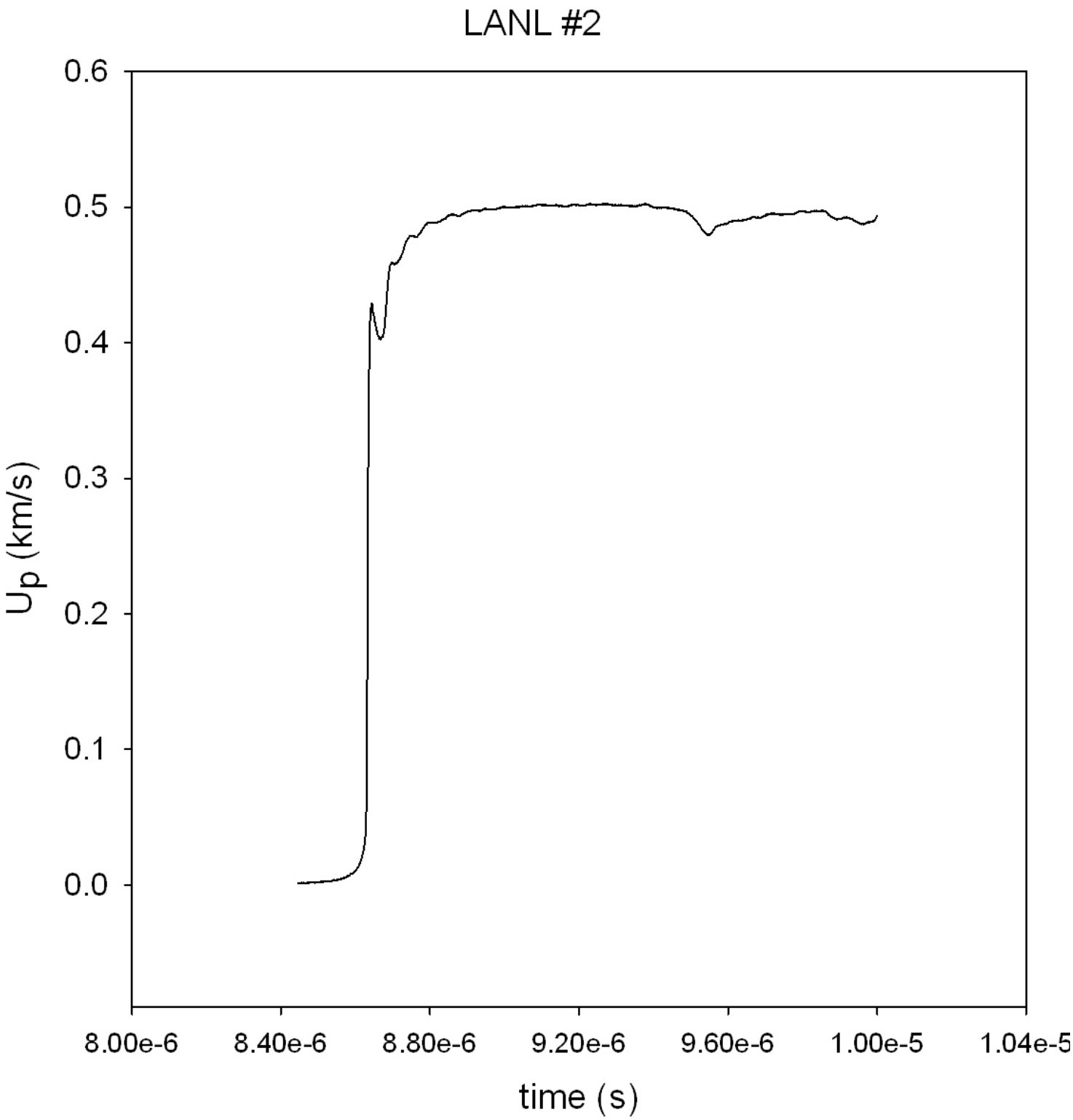
LANL #2
0.6
0.5
0.4
0.3
0.2
0.1
0.0
Up (km/s)
8.00e-6
8.40e-6
8.80e-6
9.20e-6
9.60e-6
1.00e-5
1.04e-5
time (s)

THIS PAGE INTENTIONALLY LEFT BLANK

LIST OF REFERENCES

[1] R. Ong, "Investigation of New Materials and Methods of Construction of Personnel Armour," M.S. thesis, Naval Postgraduate School, Monterey, CA, Dec 2009.

[2] C. W. Poh, "Investigation of New Materials and Methods of Construction of Personnel Armour," M.S. thesis, Naval Postgraduate School, Monterey, CA, Dec 2008.

[3] J. R. Robbins, J. L. Ding, and Y. M. Gupta, "Load Spreading And Penetration Resistance Of Layered Structures—A Numerical Study," *Int. J Impact Eng*., vol. 30(6), pp. 593–615, 2004.

[4] Y. M. Gupta and J. L. Ding, "Impact Load Spreading In Layered Materials And Structures: Concept And Quantitative Measure," Int. J Impact Eng., vol. 27(3), pp. 277–91, 2002.

[5] M. L. Wilkins, "Mechanics Of Penetration And Perforation," Int. J. Engng. Sci., vol. 16, pp. 793–807, 1978.

[6] W. Herrman, "Constitutive Equation For The Dynamic Compaction Of Ductile Porous Materials," Sandia Laboratories, Albuquerque, New Mexico, December 12, 1968. Reprinted from Journal of Applied Physics, vol. 40, no. 6, pp. 2490–2499, May 1969.

[7] C. E. Anderson, Jr., S. Chocron, and T. Behner, "A Constitutive Model for In Situ Comminuted Silicon Carbide," *Journal of the American Ceramic Society*, Vol 92, No. 6, pp. 1280–1286, 2009.

[8] C. C. Ho. "Assembly and Commissioning of Naval Postgraduate School gas gun for impact studies," M.S. thesis, Naval Postgraduate School, Monterey, CA, December 2009.

[9] Olympus, "Models 5072PR, 5073PR, 5077PR: Ultrasonic Pulser/receivers User's manual," Panametrics-NDT, Version A, March 2008.

[10] W. H. Gust and E. B. Royce, "Dynamic Yield Strengths of B4C, BeO, and Al2O3 Ceramics," *Journal of Applied Physics*, vol 42, No. 1, January 1971.

[11] D. E. Grady, "Dynamic Properties of Ceramic Materials," Report SAND94-3266, Sandia National Lab, Albuquerque, NM, February 1995.

[12] W. D. Reinhart and L. C. Chhabildas, “Strength Properties of Coors AD995 Alumina in the Shocked State,” *International Journal of Impact Engineering*, vol. 29, pp. 601–619, 2003.

[13] W. F. Hemsing, “Velocity sensing Interferometer (VISAR) modification,” Review of Scientific Instruments, vol. 50, no. 1, pp. 73–78, January 1979.

[14] T. Mashimo, Y. Hanaoka, and K. Nagayama, “Elastoplastic properties under shock compression of Al2O3 single crystal and polycrstyal,” *Journal of Applied Physics*, Vol 63, No 2, pp. 327–336, 15 January 1988.

[15] S. P. Marsh, *LASL Shock Hugoniot Data*, University of California Press, 1980.

[16] G. R. Johnson and T. J. Holmquist, “An Improved computational constitutive model for brittle materials,” American Institute of Physics, 1992.

[17] T. J. Ahrens, W. H. Gust, and E. B. Royce, “Material Strength Effect in the Shock Compression of Alumina,” *Journal of Applied Physics*, vol. 39, No. 10, September 1968.

[18] Y. Sato, S. Akimoto, “Hydrostatic Compression of 4 Corundum-Type Compounds-Alpha-Al2O3, V2O3, Cr2O3, and Alpha-Fe2O3,” *Journal of Applied Physics*, vol. 50, No. 8, 1979.

[19] Lee Davison and Mohsen Shahinpoor, “Effects of Shock Compression on Ceramic Materials,” *High Pressure Shock Compression of Solids III*, Springer-Verlag, New York, 1998.

INITIAL DISTRIBUTION LIST

1. Defense Technical Information Center
   Ft. Belvoir, VA

2. Dudley Knox Library
   Naval Postgraduate School
   Monterey, CA

3. Lee Mastroianni
   Office of Naval Research
   Washington, DC

4. Brian Jensen
   Los Alamos National Lab
   Los Alamos, NM

5. Daniel W. O'Sullivan
   United States Naval Academy
   Annapolis, MD

6. Joseph M. Denzel
   Varian Medical Systems, Inc.
   Milpitas, CA

7. Jeremy J. Denzel
   Haas Automation, Inc.
   Oxnard, CA

8. William D. Jansen
   Makago Electronics Inc.
   San Diego, CA

9. Frank Zok
   University of California at Santa Barbara
   Santa Barbara, CA